

1 Submitted to Hydrology and Earth System Sciences (HESS)

2

3 *Characterizing Coarse-Resolution Watershed Soil Moisture Heterogeneity Using Fine-*
4 *Scale Simulations*

5

6 W.J. Riley¹ and C. Shen²

7

8 ¹Earth Systems Division, Climate and Carbon Department, Lawrence Berkeley National
9 Laboratory, Berkeley, CA 94720

10 ²Department of Civil and Environmental Engineering, The Pennsylvania State
11 University, University Park, PA 16802

12

13 **Abstract.** Watershed-scale hydrological and biogeochemical models are usually
14 discretized at resolutions coarser than where significant heterogeneities in topography,
15 abiotic factors (e.g., soil properties), and biotic (e.g., vegetation) factors exist. Here we
16 report on a method to use fine-scale (220 m gridcells) hydrological model predictions to
17 build reduced order models of the statistical properties of near-surface soil moisture at
18 coarse-resolution (2^5 times coarser; ~ 7 km). We applied a watershed-scale hydrological
19 model (PAWS-CLM4) that has been previously tested in several watersheds. Using these
20 simulations, we developed simple, relatively accurate ($R^2 \sim 0.7 - 0.8$) reduced order
21 models for the relationship between mean and higher-order moments of near-surface soil
22 moisture during the non-frozen periods over five years. When applied to transient
23 predictions, soil moisture variance and skewness were relatively accurately predicted (R^2
24 $\sim 0.7 - 0.8$), while the kurtosis was less accurately predicted ($R^2 \sim 0.5$). We also tested
25 sixteen system attributes hypothesized to explain the negative relationship between soil
26 moisture mean and variance toward the wetter end of the distribution and found that, in
27 the model, 59% of the variance of this relationship can be explained by the elevation
28 gradient convolved with mean evapotranspiration. We did not find significant
29 relationships between the time rate of change of soil moisture variance and covariances
30 between mean moisture and evapotranspiration, drainage, or soil properties, as has been
31 reported in other modeling studies. As seen in previous observational studies, the
32 predicted soil moisture skewness was predominantly positive and negative in drier and
33 wetter regions, respectively. In individual coarse-resolution gridcells, the transition

1 between positive and negative skewness occurred at a mean soil moisture of $\sim 0.25 - 0.3$.
2 The type of numerical modeling experiments presented here can improve understanding
3 of the causes of soil moisture heterogeneity across scales, and inform the types of
4 observations required to more accurately represent what is often unresolved spatial
5 heterogeneity in regional and global hydrological models.
6

1 **1 Introduction**

2 Representation of the structure and dynamics of fine-scale spatial structure in
3 hydrological states and fluxes has been shown to significantly influence coarse-scale
4 surface energy budgets (e.g., ET (Wood, 1997; Wood, 1998; Vivoni et al., 2010)), runoff
5 and streamflow (Arrigo and Salvucci, 2005; Vivoni et al., 2007; Barrios and Frances,
6 2012), regional-scale feedbacks with the atmosphere (Nykanen and Foufoula-Georgiou,
7 2001), and biogeochemical responses (Dai et al., 2012; Zhang et al., 2012). It has been
8 argued that the relevant spatial scale for hydrological state and flux heterogeneity is on
9 the order of 100 m (Wood et al., 2011), while for biogeochemical dynamics it may be as
10 small as 1 m (Burt and Pinay, 2005; Groffman et al., 2009; Frei et al., 2012; McClain et
11 al., 2003). The current suite of land models representing coupled hydrological and
12 biogeochemical cycles and used for analyses of water resources and water quality (e.g.,
13 HydroGeoSphere (Li et al., 2008), CATHY (Weill et al., 2011), PIHM (Qu and Duffy,
14 2007), tRIBS (Ivanov et al., 2004), Noah-MP+CATHY (Niu et al., 2013), GSFlow
15 (Markstrom et al., 2008), LEAF-Hydro-Flood (Miguez-Macho and Fan, 2012), GEOTop
16 (Rigon et al., 2006), MIKE-SHE (McMichael et al., 2006), WEP-L (Jia et al., 2006), and
17 PAWS (Shen, 2009; Shen and Phanikumar, 2010), and regional (e.g., (Subin et al.,
18 2011)) and global (e.g., (Koven et al., 2013; Tang et al., 2013)) climate prediction are
19 typically applied at resolutions that are orders of magnitude larger than these scales.

20 Unfortunately, there are few large-scale observational datasets with which to test the
21 impact of the discrepancies in scale between model representation and known variability
22 of coupled hydrological and biogeochemical processes. This problem is particularly acute
23 for biogeochemical dynamics, which generally depend strongly on the hydrological state.

24 Watershed-scale hydrological models are often tested against, or calibrated to, stream
25 flow observations. The impact of these types of calibrations on the relative accuracy of
26 surface soil moisture heterogeneity is not well characterized. For example, Nykanen and
27 Foufoula-Georgiou (2001) used observations from the 1997 SGP experiment to
28 investigate the impact of nonlinear soil moisture dependencies of parameters on the scale
29 dependency of those parameters. They showed that failing to consider this scale
30 dependency could cause large biases in predicted surface runoff. Gebremichael et al.
31 (2009) compared scaling characteristics of spatial soil moisture fields from the same 1997

1 SGP experiment with predicted values from a distributed hydrologic model.
2 Inconsistencies between the observed and predicted soil moisture mean and spatial
3 scaling parameters indicated that while the model accurately reproduced outlet stream
4 flow the underlying mechanisms leading to runoff might have been inaccurately
5 simulated.

6 Quantifying relationships between the statistical properties of the soil moisture field
7 and spatial scale may allow prediction of heterogeneity at scales finer than those resolved
8 by the model. Since the pioneering work of Rodriguez-Iturbe (1995) and Wood (1998),
9 who described the power law decay of variance as a function of the observation scale,
10 many studies have quantified the variance-scale relationship. Hu et al (1997) showed that
11 the variance (σ_{θ}^2) of the soil moisture (θ) field at different spatial averaging areas (A) can
12 be related to the ratio of those areas raised to a scaling exponent (γ ; i.e., ‘simple scaling’).
13 They also showed that γ is related to the spatial correlation structure of the soil moisture
14 field and that it decreases as soils dry. Their scaling analysis of higher-order moments
15 indicated that soil moisture might not always follow simple scaling. A number of
16 investigators have since demonstrated that the relationship between σ_{θ}^2 and spatial scale
17 is not log-log linear across all spatial scales, and that the relationship can depend on the
18 mean soil moisture (μ_{θ}) field (e.g., (Mascaro et al., 2010, 2011; Famiglietti et al., 1999;
19 Nykanen and Foufoula-Georgiou, 2001; Das and Mohanty, 2008; Joshi and Mohanty,
20 2010)).

21 It has been further observed that soil moisture mean is often related to its variance
22 and higher-order moments. Most commonly, an upward convex relationship between μ_{θ}
23 and σ_{θ}^2 has been reported when a sufficiently large range of mean moistures is analyzed
24 (e.g., (Teuling and Troch, 2005; Lawrence and Hornberger, 2007; Teuling et al., 2007;
25 Famiglietti et al., 2008; Pan and Peters-Lidard, 2008; Brocca et al., 2010; Brocca et al.,
26 2012; Tague et al., 2010; Rosenbaum et al., 2012; Li and Rodell, 2013; Choi and Jacobs,
27 2011)). Theoretical analyses have indicated that an upward convex relationship is
28 consistent with current understanding of soil moisture dynamics (e.g., Vereecken et al.
29 (2007)).

30 Famiglietti et al. (2008) used over 36,000 soil moisture observations in four field
31 campaigns to demonstrate that soil moisture variability generally increased with extent

1 scale and followed fractal scaling. Their reported soil moisture standard deviation versus
2 mean moisture content exhibited a convex upward relationship, with the peak of their
3 best-fit relationships occurring at ~ 0.15 mean soil moisture. Brocca et al. (2012), using
4 data from 46 sites over two years in two adjacent $\sim 200 \text{ km}^2$ areas, observed a peak in the
5 convex upward relationship around 0.2-0.25 mean soil moisture. Choi and Jacobs (2011)
6 studied observations from two years of the Walnut Creek watershed, Iowa, Soil Moisture
7 Experiment (2002, 2005). They observed a convex upward relationship during the 2002
8 observations when the soil moisture range extended down to ~ 0.1 , but not in 2005 when
9 mean soil moisture did not drop below ~ 0.15 . Rosenbaum et al. (2012) concluded that the
10 relationship between the 0-5 cm soil moisture spatial standard deviation and mean also
11 had a convex up shape, but peaked at a higher mean soil moisture level (0.35-0.40),
12 although their range of mean soil moisture extended substantially further (0.58) than the
13 other studies cited above.

14 Several studies have also investigated the relationships between observed soil
15 moisture mean and higher order moments (skewness (s_θ) and kurtosis (k_θ)). For
16 example, Famiglietti et al. (1999) used observations from the SGP97 experiment to
17 conclude that the distribution of surface soil moisture content evolved from negatively
18 skewed under very wet conditions, to normal in the midrange of mean moisture, to
19 positively skewed under dry conditions. For the same SGP97 dataset, Ryu and Famiglietti
20 (2005) discussed the bimodality of the soil moisture distributions (which will be reflected
21 in k_θ), and concluded that it resulted primarily from fractional precipitation within the
22 observational footprint.

23 A fewer number of studies have combined observations of soil moisture with
24 distributed hydrological model predictions to investigate spatial scaling properties. Li and
25 Rodell (2013) examined spatial statistics of in situ, satellite-retrieved, and modeled soil
26 moisture over three large climate regions. The relationship between σ_θ^2 and μ_θ had an
27 upward convex shape for the in situ measurements, but not for the modeled relationship.
28 Manfreda et al. (2007) examined the statistical structure of soil moisture patterns using
29 modeled soil moisture obtained from the North American Land Data Assimilation
30 System (NLDAS). They concluded that σ_θ^2 followed a power law relationship with
31 averaging area and the dynamics of the relationship were controlled by mean soil water

1 content. Maxwell (2010) performed transient simulations of an arid mountain system and
2 showed that the land-energy fluxes were spatially correlated and that the soil saturation
3 vertical structure did not follow a simple scaling relationship. Ivanov et al. (2010) studied
4 the relationship between soil moisture mean and its coefficient of variation using a
5 numerical model applied to a small hillslope, and demonstrated hysteretic patterns during
6 the wetting-drying cycle. They concluded that the system response is not unique given
7 the same initial mean state, but that it depends on the magnitude of precipitation inputs.

8 The relationships between soil moisture mean and statistical moments potentially
9 depend on a wide range of factors and on spatial extent. As reviewed in Brocca et al.
10 (2007), soil moisture statistical properties can be impacted by lateral redistribution
11 (Moore et al., 1988; Williams et al., 2003), radiation (Moore et al., 1993; Western et al.,
12 1999), soil characteristics (Hu et al., 1997; Famiglietti et al., 1998; Seyfried, 1998),
13 vegetation characteristics (Qiu et al., 2001; Hupet and Vanclooster, 2002), elevation
14 above the drainage channel (Crave and GascuelOdoux, 1997), downslope gradient (Merot
15 et al., 1995), bedrock topography (Chaplot and Walter, 2003), specific upslope area
16 (Brocca et al., 2007), and landscape unit (Park and van de Giesen, 2004; Wilson et al.,
17 2004). Famiglietti et al. (1998) argued that under wet conditions, the best correlation of
18 soil moisture variability was with soil porosity and hydraulic conductivity, and under dry
19 conditions, with relative elevation, aspect, and clay content. Western et al. (1999) found
20 that during wet conditions the best predictor of the soil moisture spatial pattern was the
21 specific area (through lateral redistribution) while during dry conditions the best predictor
22 was the potential solar radiation index (through aspect and evapotranspiration). Lawrence
23 and Hornberger (2007) argued that trends across climate zones are related to the wilting
24 point and porosity.

25 Albertson and Montaldo (2003) and Montaldo and Albertson (2003) presented a
26 theoretical argument for the impact of various factors on the relationship between soil
27 moisture mean and variance. They showed that covariances between anomalies of soil
28 moisture, infiltration, drainage, and ET control the production and destruction of variance
29 over time. Teuling and Troch (2005) applied a similar approach to study the impacts of
30 vegetation, soil properties, and topography on the controls of soil moisture variance.

1 Building on these previous studies, we begin with a downscaling hypothesis that
2 consistent relationships between the transient higher-order statistical moments and mean
3 near-surface soil moisture fields exist (i.e., a ‘downscaling’ closure relationship). We
4 leave the problem of upscaling these relationships and their impact on the coarse-
5 resolution transient solution for further work. In particular, we used a five-year, high-
6 resolution hydrological simulation of the Clinton River Watershed in Michigan to
7 characterize relationships between μ_θ and σ_θ^2 , s_θ , and k_θ . Although we expected these
8 relationships to vary with depth, we only evaluated the depth interval 0-10 cm to make
9 the analysis scope tractable; future work will address this shortcoming. We also tested the
10 extent to which using discrete bins across the mean moisture range improved
11 characterization of spatial soil moisture heterogeneity. We then applied these
12 relationships to investigate hypothesized controllers of soil moisture heterogeneity as a
13 function of soil properties, evapotranspiration, topography, etc. The value of using a
14 model, compared to observations alone, for this analysis is that we have continuous and
15 spatially explicit estimates of states and fluxes, and since we know the mechanisms
16 included in the model, we can attribute patterns to individual processes.

17 In the Methods section we describe the Clinton River Watershed, the numerical
18 model we applied (PAWS-CLM), model forcing and surface characterization applied,
19 simulations performed, and our approach to generating a surrogate, or reduced order
20 (ROM), model of fine-scale soil moisture heterogeneity. In the Results and Discussion
21 section we discuss the surrogate model estimates, the value of using a binned approach to
22 characterizing soil moisture variability, and predicted controls on the relationship
23 between soil moisture mean and variance. The last section provides a brief summary and
24 conclusions.

25 **2 Methods**

26 **2.1 The Clinton River Watershed**

27 Our study domain is the Clinton River watershed (Figure 1), an 1837 km², humid
28 continental-climate basin draining into Lake St. Clair that was described in detail by Shen
29 et al. (2013b). Precipitation is relatively uniformly distributed throughout the year but
30 there is strong seasonal variation in solar radiation and air temperature that affect

1 evapotranspiration (ET) demands. This watershed is well suited for our study because of
2 its varied topography and subsurface properties, heterogeneity of surface and subsurface
3 lateral exchanges, and heterogeneity in vegetation. The basin has rugged hills on the
4 highlands of the west and flat, low-lying plains toward the east. This contrast in
5 topography, as shown later, impacts large-scale groundwater flow and the differences
6 between hilly and flat terrain soil moisture dynamics. Urban areas of varying intensity
7 span the southern portion of the watershed, the northwest is largely forested, and the
8 northeast is dominated by agriculture. Glacial drifts and lucastrine deposits in the
9 southeast form the unconfined aquifer, underlain by shale rock that bears little water.
10 High-resolution elevation (30 m), land use (30 m), soil (1:12,000 to 1:63,360 SSURGO),
11 river hydrography (1:24,000), well-log based aquifer characteristics (~1000 m), land-
12 based climate forcing data (12 stations; precipitation, temperature, humidity, and wind
13 speeds), and simulated steady state carbon and nitrogen states (220 m) are used as inputs
14 to the model (Shen et al., 2013b).

15 **2.2 PAWS-CLM4 Model Description and Simulations Performed**

16 We applied the PAWS+CLM model to generate watershed-scale predictions for the
17 analyses presented here. PAWS (Process-based Adaptive Watershed Simulator) (Shen et
18 al., 2013b; Shen and Phanikumar, 2010) is a computationally efficient, physically-based
19 hydrologic model that has recently been coupled with CLM4.0 (Lawrence et al., 2011).
20 PAWS+CLM explicitly solves the physically-based governing partial differential
21 equations for overland flow, channel flow, subsurface flow, wetlands, and the dynamic
22 two-way interactions among these components. The model evaluates the integrated
23 hydrologic response of the surface–subsurface system using a novel non-iterative method
24 that couples runoff and groundwater flow to vadose zone processes approximating the
25 three-dimensional (3D) Richards equation. By reducing the dimensionality of the fully
26 3D subsurface problem, the model significantly reduces the computational demand with
27 little loss of physics representation. We run the model with hourly time steps, but
28 aggregate the results to a diurnal time step for the analyses performed here.

29 The PAWS+CLM model has been tested extensively with analytical and 3D
30 benchmarks and compares favorably with other physically-based models (Maxwell et al.,
31 2014). It has been applied in several U.S. Midwest watersheds, including the 1140 km²

1 Red Cedar River (Shen and Phanikumar, 2010), the 1837 km² Clinton River (Shen et al.,
2 2013b), the 4527 km² Upper Grand, the 5232 km² Kalamazoon River, the 14430 km²
3 Grand River, and the 22260 km² Saginaw River basins. More recently, physically-based
4 reactive transport of nutrients and bacteria has been integrated and the model has been
5 applied to a desert environment in Southern California to evaluate groundwater
6 sustainability.

7 We applied PAWS+CLM at 220 m × 220 m horizontal resolution across the Clinton
8 River watershed. Although this resolution is coarser than the hyper-resolution called for
9 in Wood et al. (2011) and proof-of-concept work in Kollet et al. (2010), it provides
10 substantial resolution of topographic and landuse variation across a horizontal 256×280
11 grid. Twenty vertical layers were used to discretize the subsurface between the land
12 surface and bedrock top. Therefore the vertical spatial resolution varies throughout the
13 basin depending on the depth to bedrock. As described in Shen et al. (2013a), to create a
14 PAWS+CLM model for the Clinton River watershed, daily weather data were obtained
15 from the National Climatic Data Center (NCDC, 2010). We obtained 30 m resolution
16 National Elevation Dataset (NED) to generate average cell elevation and lowland storage
17 bottom elevation. The 30 m resolution IFMAP 2001 land use and land cover data
18 (MDNR, 2010) were aggregated to provide land use information. Three dominant land
19 use types (PFTs) were modeled in each horizontal cell. The soil color data is extracted
20 from a global dataset (GSDT, 2000). We obtained the spatial distribution of lateral
21 conductivities of the unconfined aquifer (glacial drift) as well as depths to bedrock by
22 interpolating well records from the WELLOGIC database (GWIM, 2006; Simard, 2007)
23 using Kriging. The bedrock has very low permeability as it is composed of shale and
24 some limestone. The model was calibrated against USGS gaging station 04165500
25 (Clinton River at Mt. Clemens) using a parallel version of the differential evolution
26 algorithm (Chakraborty, 2008). The simulations were performed from 2001 to 2008 with
27 the first three years used as model ‘spin-up’ and 2004–2008 included in our analysis. We
28 used daily-averaged top 10 cm soil moisture (θ) fields for the analyses presented here. To
29 simplify our attempt at estimating quantitative relationships between the spatial
30 properties of the fine-resolution moisture fields and the mean moisture fields, we focused
31 on the unfrozen periods during each year (days 130-300). The 2004-2008 temporal

1 average soil moisture predicted in the 220 m simulation is shown in Figure 1. There is a
2 large-scale spatial pattern in the soil moisture field, being generally higher on the eastern
3 lowland plains than on the western hills, due to basin-scale groundwater flow. However,
4 contrary to the coarser-resolution soil moisture map provided previously (Figure 10d in
5 Shen et al. (2013b)), Figure 1 shows fine-scale features, e.g., high surface moisture near
6 channels and high moisture in clayey soils near the eastern boundary.

7 **2.3 Developing Surrogate Models for Surface Soil Moisture Moments**

8 We developed two classes of simple surrogate models to represent soil moisture
9 spatial heterogeneity as a function of mean soil moisture in coarse-resolution gridcells.
10 We chose a factor of 2^5 in resolution to define the coarse-resolution gridcells, resulting in
11 thirty-four 7040 m coarse-resolution gridcells across the watershed. The first class of
12 surrogate model was separate polynomials describing the relationships between μ_θ and
13 σ_θ^2 , s_θ , and k_θ for each coarse-resolution gridcell. We tested the impact on the accuracy
14 of the relationship for best-fit 1st, 2nd, and 3rd order polynomials. The second class of
15 surrogate model represents the fraction of high-resolution gridcells in each coarse-
16 resolution gridcell that fall into a particular mean soil-moisture bin. A disadvantage of
17 this latter approach is that it is not as easy to mathematically synthesize the patterns,
18 while a potential advantage is that it represents the probability distribution function of the
19 moisture even in the case where the first few statistical moments do not fully capture its
20 properties.

21 **2.4 Relationships between Soil Moisture Heterogeneity and System Properties**

22 We investigated the relationship between daily σ_θ^2 and μ_θ over the μ_θ range where σ_θ^2
23 decreases with increasing μ_θ . As shown below, most of the μ_θ predictions were above the
24 ~ 0.2 breakpoint (as often observed and predicted here) for the peak of a convex-up
25 relationship between σ_θ^2 and μ_θ . Therefore, many of the coarse-resolution gridcells were
26 relatively well characterized by a linear fit with a negative slope, although about 20% of
27 the gridcells were predicted to have a full convex-up relationship. For the latter gridcells,
28 we evaluated the best-fit slope for the portion of the data to the wetter side of the peak of
29 the convex-up relationship.

1 We investigated sixteen hypothesized controllers of this slope (based on the literature
2 cited in the Introduction), all of which are represented explicitly or implicitly in
3 PAWS+CLM: specific upslope area, gradient, variance of the gradient in each coarse-
4 resolution gridcell, aspect, soil characteristics (porosity, clay content, conductivity),
5 temporal mean evapotranspiration ($\overline{E_T}$ (W m^{-2})), temporal variance in $\widehat{E_T}$, bedrock
6 topography, temporal mean groundwater depth ($\overline{G_w}$ (m)), temporal variance in
7 groundwater depth ($\widehat{G_w}$ (m)), elevation, mean surface roughness, variance in roughness,
8 and stream drainage density. We used TopoToolbox (Schwanghart and Kuhn, 2010) to
9 evaluate the topographic indices used in the analysis.

10 **3 Results and Discussion**

11 **3.1 Comparing Model Predictions to Observations**

12 PAWS+CLM has been extensively tested and demonstrated favorable comparisons
13 with various observations from several basins (Shen et al., 2013b; Shen and Phanikumar,
14 2010; Niu and Phanikumar, 2012). In the Clinton River watershed, the model has been
15 shown to satisfactorily reproduce streamflow observations both at the basin outlet and
16 uncalibrated inner gages (Nash-Sutcliffe model efficiency coefficient ~ 0.65), spatially
17 distributed water table depths ($R^2=0.66$), soil temperature, and MODIS satellite-based
18 observations of Leaf Area Index (LAI) and evapotranspiration (ET) (Shen et al., 2013b).
19 In other basins, PAWS+CLM was able to match observed transient water table depths
20 from a USGS monitoring well and water storage anomalies measured by the GRACE
21 satellite.

22 In addition to the comparisons described above, we compared simulated versus
23 observed soil moisture at a site in Romeo, MI from an Enviro-weather Automated
24 Weather Station Network (Figure 2). Since maintenance records indicated problems with
25 the soil moisture sensor installation in 2008, we only show comparisons in 2009. The
26 winter freeze-up at the beginning of 2009, shown as a period of very low soil moisture,
27 was well captured by the model. The subsequent large variations due to freeze and thaw
28 were also closely reproduced, with some over-estimation near the end of the freezing
29 cycle (early April 2009). In May, soil moisture was over estimated during the recession
30 periods after storms. In late Spring, plants may preferentially increase rooting density

1 near the surface when there is high moisture content, leading to a stronger recession of
2 near-surface moisture (Sivandran and Bras, 2013). However, the current static rooting
3 algorithm in CLM cannot reproduce this mechanism, and therefore may be partly
4 responsible for this bias. From June to November the model accurately predicted the
5 mean, range of fluctuations (0.25~0.34), and general trend. However, toward the end of
6 the year, the predicted freeze-up was not present in the observations. These mismatches
7 may be attributed to differences between grid average moisture of a 220 m cell and the
8 site-specific moisture measured by the probe or local variation and uncertainty in
9 subsurface properties.

10 **3.2 Predicted Mean Moisture**

11 The range and dynamics of predicted mean moisture at the coarse-resolution varied
12 substantially across the watershed (Figure 1; Figure 3). The western upland gridcells
13 tended to be drier overall with the mean moisture increasing toward the east and south,
14 which are lower elevation gridcells receiving both surface and sub-surface water inputs.
15 The low precipitation inputs in 2006 had proportionally larger impacts in the wetter,
16 eastern gridcells, resulting in up to 25% decreases in mean saturation.

17 **3.3 Relationships Between Soil Moisture Mean and Higher-Order Moments**

18 Using the 0-10 cm soil moisture predictions from the 220 m resolution simulation, we
19 evaluated μ_θ , σ_θ^2 , s_θ , and k_θ at every time point (daily) for each of the thirty-four
20 7040 m \times 7040 m coarse-resolution gridcells (Figure 4 shows representative transient
21 profiles for one subregion over 90 d of the simulation). We used these temporally
22 resolved values to build 1st, 2nd, and 3rd order best-fit polynomial relationships, with the
23 3rd order fits having generally the best predictive power and therefore applied in the
24 remainder of our analysis. Overall, these surrogate models accurately captured the
25 relationships between μ_θ and σ_θ^2 , s_θ , and k_θ , with mean R^2 values of 0.73, 0.74, and
26 0.75, respectively.

27 Different types of $\sigma_\theta^2 \sim \mu_\theta$ relationships were predicted among the thirty-four coarse-
28 resolution gridcells across the watershed. Some gridcells exhibited large, negative slopes
29 with little scattering, e.g., #10, #17, #40, # 41, indicating that soil moisture heterogeneity
30 in these cells was strongly controlled by mean moisture, and that the variability was

1 smallest on the wettest days. Some cells have much smaller slopes, e.g., #6, #7, #22 and
2 #23, suggesting that their variability was less sensitive to mean moisture. These cells
3 tended to have very small spatial variability throughout the year. Most gridcells with
4 monotonic $\sigma_{\theta}^2 \sim \mu_{\theta}$ relationships did not experience mean moisture below ~ 0.25 .
5 However, for some (e.g., gridcells #10, #17, #24), this monotonic, approximately linear
6 relationship extended down to $\mu_{\theta} \sim 0.2$. We did not observe any gridcells with a purely
7 upward $\sigma_{\theta}^2 \sim \mu_{\theta}$ slope. On the other hand, about 20% of the gridcells had convex up $\sigma_{\theta}^2 \sim$
8 μ_{θ} relationships (e.g., gridcells #19, #26, #32 and #3). These gridcells primarily reside in
9 the large topographic gradient in the middle of the watershed that alternates between
10 recharge and discharge across the year (Salvucci and Entekhabi, 1995; Shen et al., 2013b)
11 and correspond with relatively higher drainage densities (Figure 6). Higher drainage
12 density corresponds to larger topographic variation, and this region connects upland hills
13 and lowland plains and is characterized by a sharp change in elevation. As a result it is
14 also a transition zone over which the distance to the water table decreases strongly.
15 Therefore the 7040 m cells in these regions all included large variations in soil moisture,
16 and they shift from high to low water table regimes seasonally. The differences in these
17 relationships indicate that at the 7040 m \times 7040 m scale, the $\sigma_{\theta}^2 \sim \mu_{\theta}$ relationships are
18 determined locally, a finding consistent with that by Mascaro et al. (2010), where
19 coefficients in a predictive formula for scaling exponents were related to local attributes.

20 For a particular coarse-resolution gridcell, the scattering of the $\sigma_{\theta}^2 \sim \mu_{\theta}$ points around
21 the polynomial fit, or departure from a deterministic function, can be attributed to
22 different hydrologic processes that similarly affect the mean but differently affect the
23 spatial heterogeneity. For example, homogeneous precipitation increases surface moisture
24 evenly across the domain, and therefore decreases the variance. This homogenizing effect
25 acts as the major driver that sets the negative slope in the $\sigma_{\theta}^2 \sim \mu_{\theta}$ curves. However, an
26 increase in regional groundwater flow would create spatial heterogeneity that adds to the
27 variance. This effect is clear in the transition zones (e.g., gridcells #19, #26). A
28 floodwave that inundates riparian zones (which are represented in PAWS+CLM) would
29 increase the mean soil moisture and spatial heterogeneity in the gridcell by increasing soil
30 moisture only in the riparian zones. Gridcells that are further to the west have smaller σ_{θ}^2

1 ranges for particular values of μ_θ , and have soil moisture that are less impacted by
2 exfiltration.

3 As mentioned above, Famiglietti et al. (2008) used data from several ground-based
4 measurement campaigns in the Southern Great Plains and Iowa to characterize
5 relationships between μ_θ , σ_θ^2 , and s_θ . They found convex up relationships between σ_θ^2
6 and μ_θ at 800 m and 50 km scales with a mean moisture range between $[-0.05, 0.4]$, and
7 fit an exponential function to the standard deviation: $\sigma_\theta = k_1\mu_\theta \exp(-k_2\mu_\theta)$. For the
8 range of mean moisture we predicted in the Clinton Watershed $[-0.2, 0.45]$ (i.e., a
9 smaller range than used in the Famiglietti et al. (2008) study), the overall monotonically
10 declining trend in σ_θ^2 with μ_θ qualitatively matched the trend they reported (lower left
11 panel of Figure 5). There were, however, gridcells with higher variance that did not fit
12 this pattern (i.e., #19, #26, #33). We calculated k_1 (1.3 ± 0.3) and k_2 (7.1 ± 1.0) across the
13 7040 m coarse-resolution gridcells and found a mean R^2 for all the gridcells of 0.48.
14 These predicted values of k_1 and k_2 matched well those reported by Famiglietti et al.
15 (2008) for their 1.6 km scale (1.2 and 7.1, respectively). We note also that the 3rd order
16 polynomial fit explained more of the variance of the modeled relationships than did the
17 exponential relationship, but we are not aware of a mechanistically-based rationale for a
18 choice of this relationship.

19 The relationships between μ_θ and s_θ also varied across the watershed (Figure 7). For
20 the gridcells toward the west (in the four western columns), which are typically drier than
21 those to the east, s_θ was predominantly positive across the mean moisture range,
22 implying a consistently right-skewed probability density function. The transition between
23 positive and negative s_θ occurred in several of these gridcells at μ_θ of about 0.3 – 0.35
24 (#4, #10, #17). For the wetter gridcells to the east (column 5 – 7), the μ_θ distribution was
25 predominantly left-skewed (i.e., $s_\theta < 0$), even though part of the μ_θ range was drier than
26 the transition values for the gridcells farther to the west. For the sixth and seventh column
27 (farthest east), μ_θ was predicted to be above 0.3 for the entire simulation period, and most
28 of these gridcells (and those in the southern portion of column 5) showed a decreasing s_θ
29 with increasing μ_θ . This pattern is consistent with the fact that there is a maximum μ_θ
30 value possible (corresponding to fully saturated), and as more of the 220 m gridcells
31 reach this level the probability density function becomes more left skewed.

1 Comparing our predictions (lower left panel of Figure 7) to the 800 m and 50 km s_θ
2 relationships with μ_θ reported in Famiglietti et al. (2008) indicates good qualitative
3 agreement: a monotonic decrease from positive s_θ values between 0 and 1 at μ_θ of ~ 0.2
4 to a s_θ value of between about -1 and -2 at μ_θ of ~ 0.4 . In our predictions, and somewhat
5 visible in the Famiglietti et al. (2008) observations, there is a divergence of s_θ values
6 toward the wetter end of the μ_θ range. The best linear fit to these predictions had a slope
7 of -13 and intercept of 4.2, which corresponded well to values inferred from their
8 observations at the 1.6 km scale. However, the slope and intercepts inferred from their
9 observations varied substantially and inconsistently across scale, making this comparison
10 inconclusive.

11 The relationships between predicted k_θ and μ_θ (Figure S1) can be divided into a few
12 characteristic shapes: (1) monotonically increasing (e.g., #11, 27, 34, 41); (2) relatively
13 constant (e.g., #18, 23); and (3) convex down (e.g., #13, 14, 20). To the extent that k_θ
14 represents an index of ‘peakedness’ in the moisture distribution, an increase in k_θ with
15 increasing mean moisture is consistent with the limit in the range occurring at full
16 saturation, and with s_θ becoming more negative in this part of the range. The more
17 strongly convex down shapes occur in gridcells where the mean soil moisture range
18 extends toward fully saturated, so the relationships that are more constant with μ_θ
19 variations may simply be a result of that gridcell not experiencing periods with higher μ_θ .

20 Finally, we also tested our results against the theoretical predictions of Montaldo and
21 Albertson (2003), who concluded that the time derivative of the root-zone soil moisture
22 variance ($\frac{\partial \sigma_\theta^2}{\partial t}$) would increase as the covariance between soil moisture and infiltration
23 increased, or decrease as the covariance between soil moisture and either drainage or
24 transpiration increased. We tested these potential dependencies by comparing our
25 predicted values of $\frac{\partial \sigma_\theta^2}{\partial t}$ to $\overline{\theta'K'}$, $\overline{\theta'q_r'}$, and $\overline{\theta'E'}$, where K is the soil hydraulic
26 conductivity (which affects infiltration), q_r is the drainage flux, E is the
27 evapotranspiration, the prime represents anomalies compared to the spatial mean of that
28 variable, and the overbar represents a spatial average. We evaluated these relationships
29 with daily, weekly, and monthly averaging periods using the model predictions and found
30 very weak relationships. These results indicate that the creation and destruction of

1 variance in a watershed model that represents a range of moisture redistribution
2 mechanisms is more complex than can be represented by these inferred dependencies.

3 **3.4 Predicted Soil Moisture PDF as a Function of Mean Moisture**

4 Because σ_{θ}^2 , s_{θ} , and k_{θ} of the soil moisture field do not fully characterize the
5 probability distribution function, we also examined the dependence of the proportion of
6 high-resolution gridcells in each coarse-resolution gridcell occupying μ_{θ} bins (e.g., seven
7 bins are shown in Figure 8). The advantages of this binning approach are that it more
8 fully represents the heterogeneity in μ_{θ} and allows visualization of variation within-
9 coarse-resolution gridcells.

10 An interesting observation from Figure 8 is that the coarse-resolution gridcells that
11 have a clear convex up shape for variance versus mean moisture have the peak of that
12 distribution very close to where the 3rd and 4th quartile bands have equal representation
13 (not shown). Thus, when the coarse-resolution gridcell has more of its fine-scale soil
14 moisture mean values occupying the wettest quartile, the system variance begins to
15 decline as mean moisture increases. In the gridcells that have a monotonically decreasing
16 relationship, the transition between 3rd and 4th quartile mean moisture bands occurs to the
17 drier end of the μ_{θ} range.

18 It is also interesting to note the different behavior of the wettest bin (the gray line). In
19 many of the drier cells in the upland area (e.g., #23, #24, #10), this bin remains relatively
20 constant across the μ_{θ} range. This pattern likely occurs because these regions have larger
21 topographic variation and are effective at redistributing moisture, therefore preventing the
22 wettest areas (or source areas (Lyon et al., 2004; Dunne and Black, 1970; Frankenberger
23 et al., 1999)) from expanding in area. In many cells on the western plains (e.g., #27, #28,
24 #40, #47), there appears to be a threshold soil moisture value, around 0.35, above which
25 the wettest bin suddenly grows very rapidly as mean moisture increases. This rapid
26 change is due to the upper limit of saturation set by soil porosity and the flatter terrain.

27 **3.5 Relationships between Soil Moisture Heterogeneity and System Properties**

28 As mentioned in the Introduction, many of the convex up relationships reported in the
29 literature appear to have a peak in this relationship at μ_{θ} of ~ 0.2 , although that value is
30 not universal (e.g., Rosenbaum et al. (2012)). This transition point represents the

1 transition between system properties (e.g., roughness, hydraulic conductivity) and fluxes
2 (e.g., evapotranspiration) that tend to homogenize soil moisture versus those that lead to
3 more heterogeneity. For example, imagine a flat region with a distribution of plants of
4 equal potential evapotranspiration but with drought tolerances that are different functions
5 of soil moisture (Figure S2 shows an example using CLM4.5's estimate of water stress
6 on photosynthesis (β_t) for soils with different sand composition). A precipitation event
7 that occurs on a dry coarse-resolution gridcell would tend to alleviate the drought stress
8 in a fraction of the plants, thereby leading to a higher heterogeneity in soil moisture (and
9 therefore σ_θ^2). If the precipitation continued and μ_θ increased to a level where none of the
10 plants were stressed, the now relatively more homogeneous evapotranspiration would
11 tend to reduce σ_θ^2 . As discussed in the Methods, many controllers of these tradeoffs have
12 been inferred from observations, and include topographical features, evapotranspiration,
13 and edaphic properties.

14 Because most of the coarse-resolution gridcells in our computational domain did not
15 experience μ_θ below ~ 0.2 , we investigated the relationship between σ_θ^2 and μ_θ over the
16 range where σ_θ^2 decreases with increasing μ_θ . In our predictions, $\sim 80\%$ of the coarse-
17 resolution gridcells were relatively well characterized by a linear fit with a negative slope.
18 For the remaining $\sim 20\%$, we evaluated the best-fit slope for the portion of the data to the
19 wetter side of the peak of the convex-up relationship.

20 Of the sixteen hypothesized controllers of this slope (m) that we investigated (see
21 Methods), six had independent linear best-fits with $R^2 > 0.05$: gradient (g ; $R^2 = 0.07$),
22 mean of evapotranspiration ($\overline{E_T}$ (W m^{-2}); $R^2 = 0.16$), temporal mean of the spatial
23 variance of evapotranspiration ($R^2 = 0.05$), porosity ($R^2 = 0.08$), mean of groundwater
24 depth ($R^2 = 0.06$), and mean of stream density ($R^2 = 0.05$). Using a stepwise linear
25 regression with these six variables and allowing for first order interactions, the best-fit
26 model explained 59% of the variance in m and had the form: $C_1 + C_2 g \overline{E_T}$, where C_1 and
27 C_2 are constants. Thus, over the five years of simulation, the rate at which σ_θ^2 declined
28 with increasing μ_θ was controlled primarily by the elevation gradient convolved with the
29 temporal mean of evapotranspiration. In this relationship, increases in this product leads
30 to less negative values of m (i.e., less sensitive response of σ_θ^2 to variations in μ_θ). The
31 larger the gradient and higher the evapotranspiration in the gridcell, the lower the

1 response of soil moisture spatial heterogeneity to mean soil moisture. This conclusion is
2 consistent with the ideas that (1) high evapotranspiration gridcells are more likely to be
3 those with lower likelihood of partial water stress limitation and (2) the high gradient
4 gridcells more efficiently mix surface water thereby reducing soil moisture gradients.

5 **3.6 Applying the Simple Surrogate Models to Predict Fine-Scale Heterogeneity**

6 We also evaluated whether the simple polynomial surrogate models can be used to
7 predict dynamic variations in σ_θ^2 , s_θ , and k_θ given variations in μ_θ . For this exercise, we
8 used the first three years of the simulations to train the 3rd order polynomial surrogate
9 model. We then applied those surrogates across the five years of simulation to evaluate
10 estimates for σ_θ^2 , s_θ , and k_θ within each coarse-resolution gridcell and compared those
11 estimates to the moments calculated directly from the fine-resolution simulation.

12 The surrogate-estimated values of σ_θ^2 over time corresponded well to those from the
13 fine-scale solution, with an R^2 value of 0.78 and mean absolute bias of 0.00014 (Figure
14 9). The estimates relatively accurately captured several of the dominant transients that
15 occurred, including during the 2006 drought in, e.g., gridcells #26, #27, and #28. These
16 gridcells span a μ_θ gradient from relatively drier to wetter, and that transition is apparent
17 in the σ_θ^2 gradient across these gridcells (from a value ~ 0.001 to ~ 0.006). The temporal
18 dynamics during drying are also different between these gridcells; e.g., during 2006 the
19 response in gridcell #26 is a reduction in σ_θ^2 , while in gridcells #27 and #28 the response
20 is an increase in σ_θ^2 . This differential response occurred because gridcells #27 and #28
21 had μ_θ that was high enough before the drought that, even though they dried, remained to
22 the right of the peak in the convex up relationship between σ_θ^2 and μ_θ . In contrast,
23 gridcell #26 had a μ_θ value before the drought that was close to the peak in that
24 relationship and the reduction in μ_θ therefore resulted in a reduction in σ_θ^2 .

25 The surrogate-estimated values of s_θ over time corresponded well to those from the
26 fine-scale solution, with an R^2 value of 0.74 and mean absolute bias of 0.11 (Figure 10).
27 The temporal variability in s_θ was largest in the coarse-resolution gridcells in the eastern
28 (wetter) portion of the watershed, and in particular, during 2006 as the soils dried. During
29 this period, for example, s_θ in gridcells #27 and #28 increased rapidly in Spring and then
30 stabilized at a value near zero, indicating a relatively uniform distribution of μ_θ .

1 Interestingly, the relatively drier gridcell #26 did not have as strong a response in s_θ , but
2 all three gridcells stabilized at values indicating a more uniform μ_θ distribution.

3 The polynomial surrogate model for k_θ was less accurate than those for either s_θ or
4 μ_θ , with an R^2 value of 0.51 and mean bias of 0.43 (Figure S3). In contrast to the s_θ
5 dynamics, k_θ was relatively temporally variable in both the western (e.g., gridcells #15,
6 #29) and eastern portions of the watershed. In most years in many of the wetter
7 southeastern gridcells there was a reduction in k_θ (i.e., a flattening of the μ_θ pdf)
8 following the spring thaw followed by periodic increases associated with precipitation
9 events. In contrast, during the 2006 dry period, the southeastern wetter gridcells showed a
10 reduction that was sustained over the summer.

11 **4 Limitations and Future Work**

12 Many factors impact near-surface soil moisture heterogeneity in watersheds;
13 characterizing this heterogeneity and its relationships with the mean moisture field,
14 topographical features, vegetation, and climate forcing could improve regional to global-
15 scale estimates of surface energy and greenhouse gas exchanges (which depend on soil
16 moisture). The approach we applied here, using a tested high-resolution numerical model,
17 showed promise in this regard, yet a number of limitations remain for future work. For
18 example, we did not consider the temporal pattern of the relationships. We note, though,
19 that we did not observe hysteresis in the relationships between the mean moisture field
20 and higher-order moments, as has been reported previously (Ivanov et al., 2010; Vivoni
21 et al., 2010). The high-dimensional state space, especially the influence of vertical soil
22 moisture profiles, also needs to be examined in detail. We also considered only one
23 watershed over a relatively short (five-year) period. A longer study, covering several
24 decades, would better capture the inter-annual range in precipitation and vegetation status
25 (and therefore soil moisture) that the watershed experiences. Repeating the analyses
26 described here for other watersheds with different topography, vegetation, bedrock
27 features, soil properties, etc., could yield insights on the impacts these various properties
28 have on soil moisture heterogeneity and its relationship with mean soil moisture. Such an
29 analysis could also be used to test the extent to which relationships developed in one
30 watershed could be used for other watersheds, and more specifically, for which watershed
31 features such an extrapolation would be appropriate. We also note that soil moisture

1 heterogeneity exists at scales much smaller than we simulated here (220 m), including
2 down to the soil macropore scale, where the soil biogeochemical transformations that
3 impact ecosystem function and climate occur. Further computational and data
4 enhancement that examine variability at hyper-resolution (on the order of 10 m) are the
5 next reasonable steps and are possible with current computational resources. Developing
6 modeling structures that account for, at some level, this wide range of scales will be
7 important for consistently representing terrestrial ecosystem processes.

8 Finally, an important application of the relationships developed here would be to
9 apply them with coarse-resolution simulations to substantially reduce computational costs
10 for regional and global simulations. Comparisons between fine and coarse-resolution
11 simulations of a particular watershed have been used to transfer nonlinearity from
12 microscale to mesoscale models via non-stationary effective parameters (Barrios and
13 Frances, 2012). The approach we envision here would combine that type of model
14 calibration with a cost function that includes a larger suite of observations, including the
15 ability to capture the fine-scale predicted soil moisture heterogeneity and its relationship
16 with mean moisture.

17 **5 Summary and Conclusions**

18 We applied a watershed-scale hydrological model (PAWS+CLM4) that has been
19 previously tested in the Clinton River watershed in Michigan to investigate relationships
20 between fine-scale near-surface soil moisture mean and spatial heterogeneity. We used
21 fine-resolution (220 m) simulations to calculate statistical properties of soil moisture at a
22 resolution 2^5 times coarser (~ 7 km), and then (1) developed and evaluated simple
23 polynomial surrogate models relating soil moisture mean to its variance, skewness, and
24 kurtosis during the non-frozen portion of five years; (2) applied those surrogates over the
25 time period to evaluate their accuracy; and (3) investigated the relationship between the
26 predicted soil moisture mean and variance and topographic and hydrological system
27 properties.

28 The surrogate models accurately reproduced the relationships between the soil
29 moisture mean and higher order moments ($R^2 \sim 0.7-0.8$). Driving the surrogate model
30 with the mean coarse-resolution soil moisture predictions across the simulation period
31 gave comparably accurate predictions for variance and skewness, and a less accurate (R^2

1 ~ 0.5) prediction of kurtosis. This close correspondence between the surrogate and fine-
2 resolution model predictions argues that these types of reduced order models can be used
3 to inform heterogeneity at scales below those explicitly represented at coarse resolution.
4 It also argues that the surrogates can be effectively applied to understand controls on
5 spatial heterogeneity of soil moisture, as discussed below.

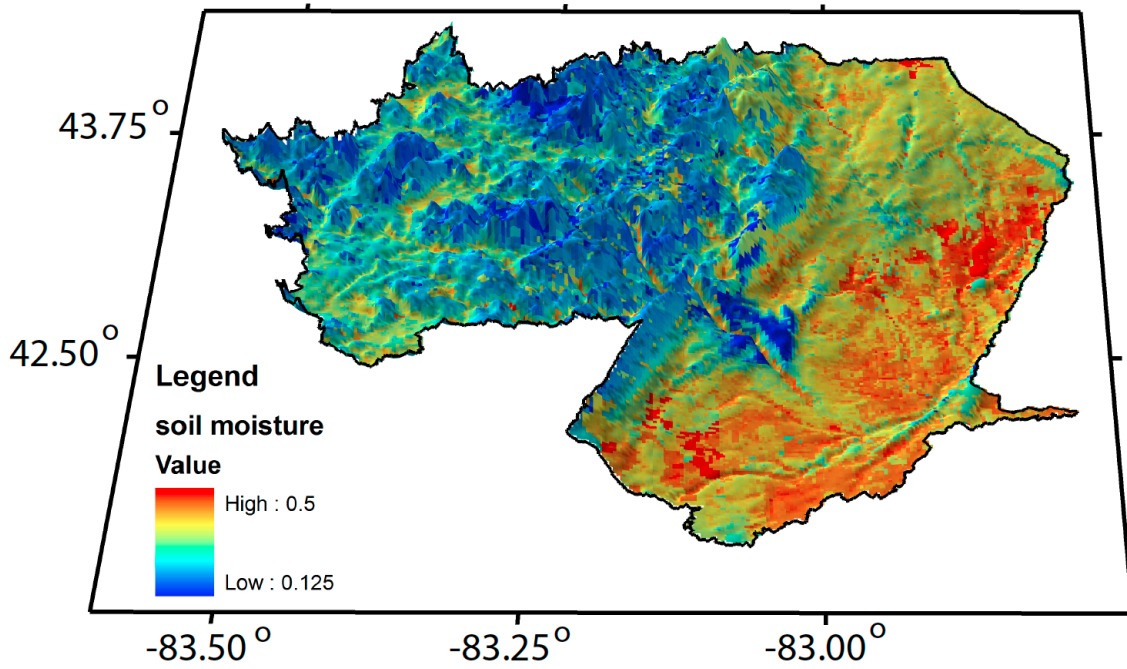
6 In our predictions, and in many reported observations, there is typically a reduction in
7 soil moisture variance with increasing mean past a particular intermediate value of the
8 mean. Many possible controllers of this relationship have been hypothesized; in our
9 predictions the approximately linear relationship was estimated ($R^2 = 0.59$) using only the
10 elevation gradient convolved with the mean of evapotranspiration in the coarse-resolution
11 gridcell. Increases in the elevation gradient and mean evapotranspiration each, and even
12 more strongly in combination, caused a shallower slope in the soil moisture mean versus
13 variance relationships. An explanation for this pattern is that high evapotranspiration
14 gridcells are more likely to be those with lower likelihood of partial water stress
15 limitation and the high gradient gridcells more efficiently mix surface water. However,
16 because we inferred these patterns from a full-complexity model with multiple interacting
17 processes, we believe carefully designed modeling experiments that isolate in turn the
18 various processes will be helpful for better understanding the controls on these
19 relationships. We conclude that these types of experiments can improve understanding of
20 the causes of soil moisture heterogeneity across scales, and inform the types of
21 observations required to more accurately represent what is often unresolved spatial
22 heterogeneity in regional and global hydrological and biogeochemical models.

23
24 *Acknowledgements.* This research was supported by the Director, Office of Science,
25 Office of Biological and Environmental Research of the US Department of Energy under
26 Contract No. DE-AC02-05CH11231 as part of their Regional and Global Climate
27 Modeling Program; and by the Next-Generation Ecosystem Experiments (NGEE Arctic)
28 project, supported by the Office of Biological and Environmental Research in the DOE
29 Office of Science under Contract No. DE-AC02-05CH11231. Shen was supported by
30 Office of Biological and Environmental Research of the US Department of Energy under
31 Contract No. DE-SC0010620. Cartographical help from Kuai Fang and Xinye Ji is
32 appreciated.

33

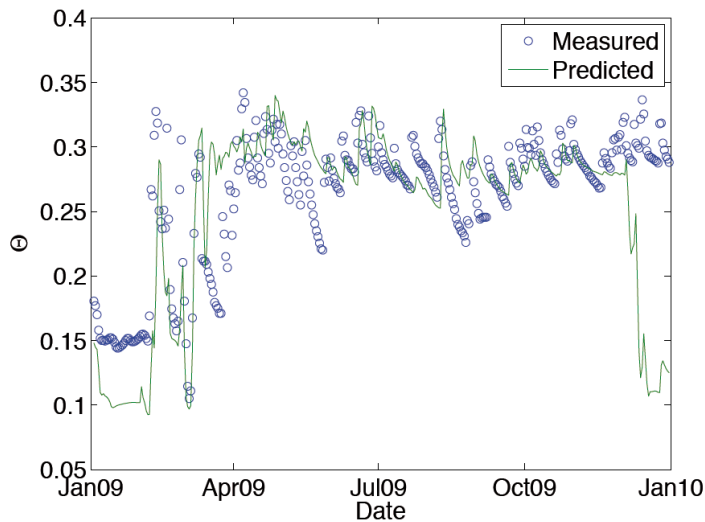
1 **6 Figures**

2
3



4
5
6
7
8
9

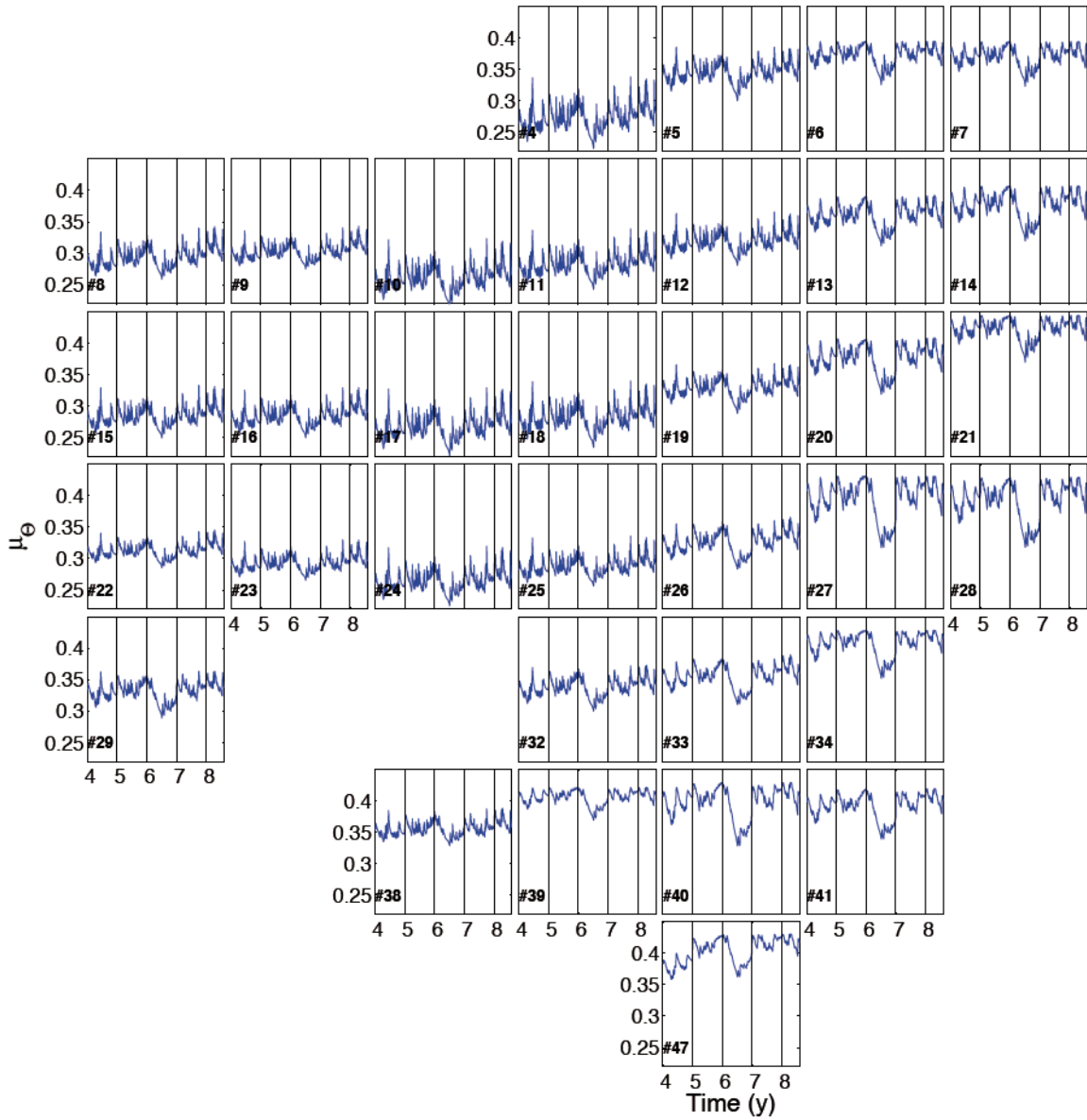
Figure 1. Topography and predicted 2004-2008 temporal average soil moisture of the Clinton River watershed (the black line outlines the watershed). The 3D elevation and shading represent the digital elevation model, which is enhanced by a 1:50 ratio, and the color represents the average soil moisture.



10
11
12
13
14

Figure 2. Comparison between 220 m resolution predicted and measured soil moisture for a site in Romeo, MI. The large differences in December 09 are caused by the model predicting freezing in the top 10 cm of soil, while the observations suggest unfrozen conditions.

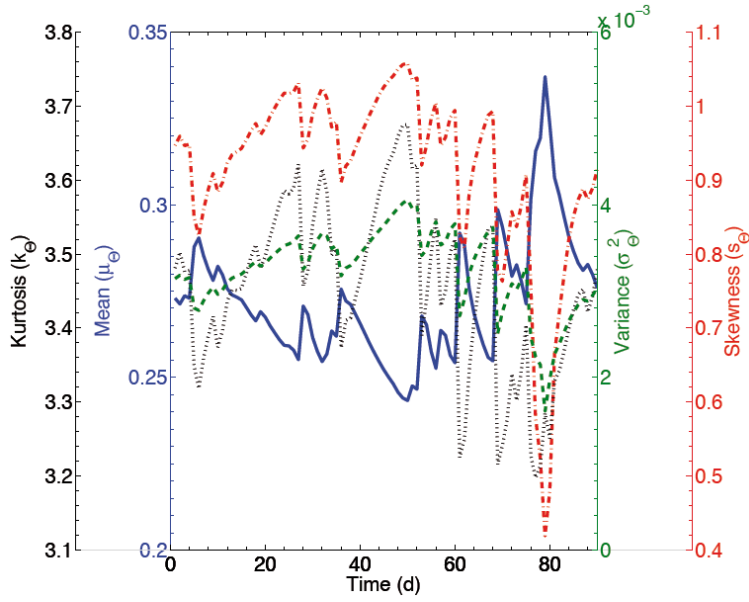
[plot_obs_pred_moisture.m]



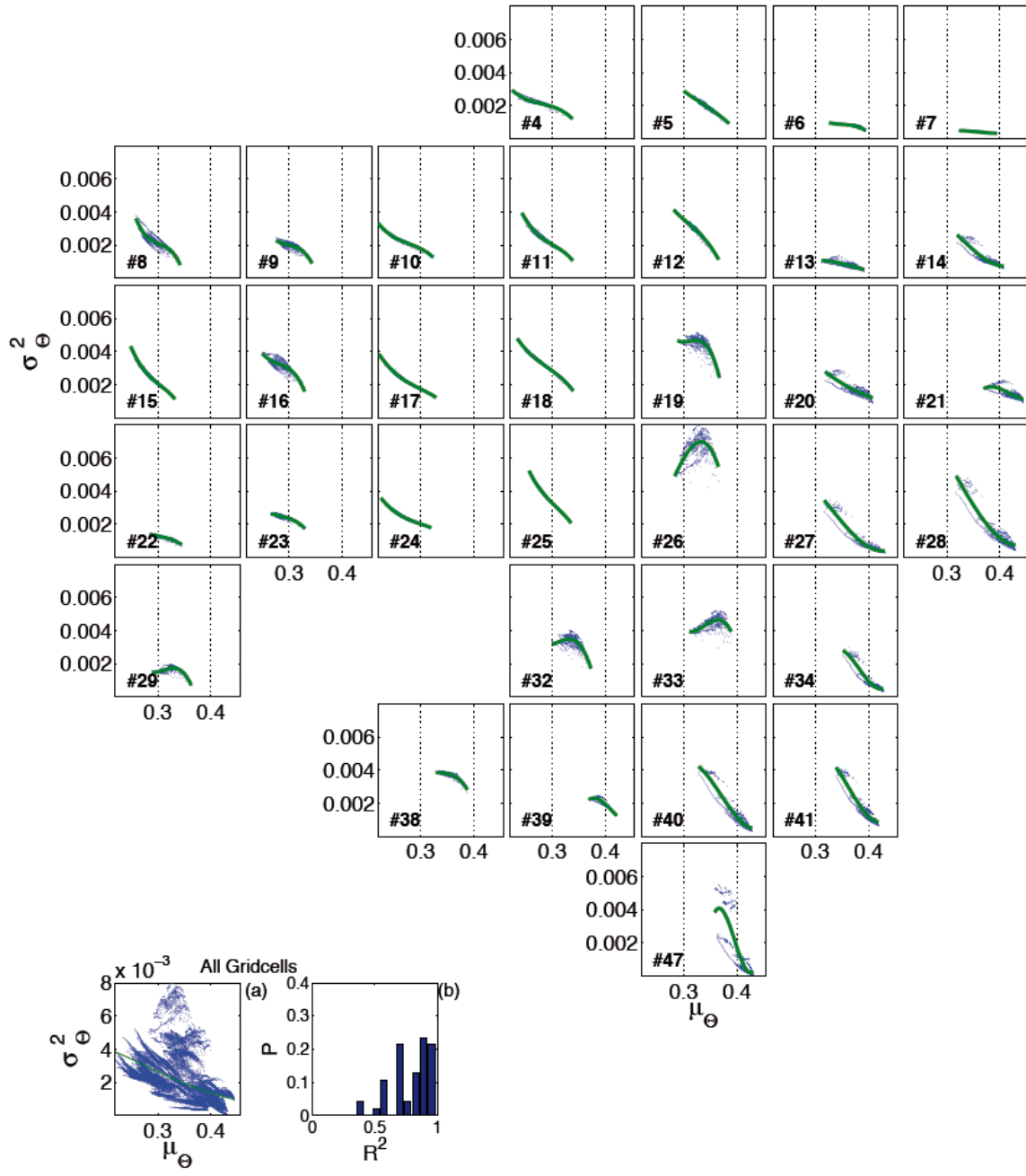
2
3
4
5
6
7

Figure 3. Fine-resolution (220 m) simulated 0 – 10 cm soil moisture mean (μ_{θ}). The individual plots are distributed in the same pattern as the coarse-resolution gridcell they represent in the watershed (see watershed boundary in Figure 1).

[model_moisture_zones_using_coarse_gridcells.m]

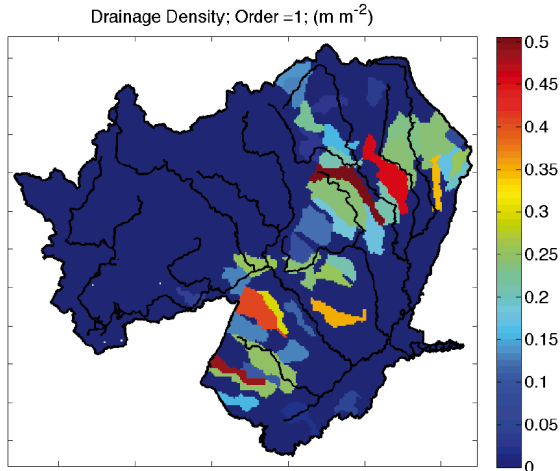


1
 2 Figure 4. Example 90-day soil moisture mean (μ_θ ; blue solid line), variance (σ_θ^2 ; green
 3 dashed line), skewness (s_θ ; red dashed-dotted line), and kurtosis (k_θ ; black dotted line)
 4 for gridcell #26. [plot_mean_moments_vs_time.m]
 5

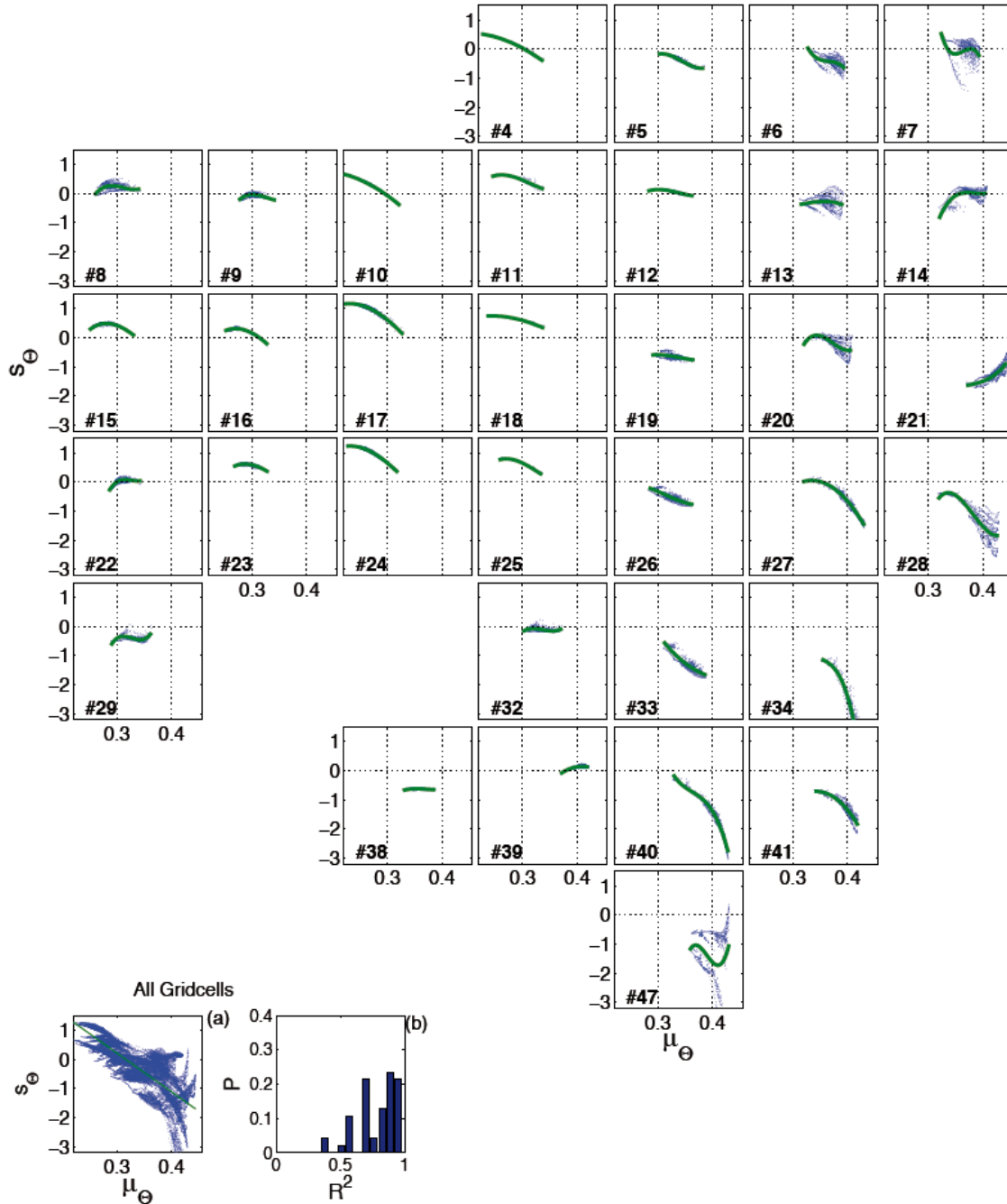


1
 2 **Figure 5.** In each subplot (except for the two in the bottom left hand corner), soil moisture
 3 variance (σ_{θ}^2) is plotted versus mean (μ_{θ}) for that coarse-resolution gridcell based on the
 4 fine-resolution (220 m) model predictions (blue dots) and the best-fit 3rd order polynomial
 5 fits (green line). The individual 7040 m coarse-resolution gridcells are placed in their
 6 relative position in the watershed. Bottom left hand corner: (a) Soil moisture variance (σ_{θ}^2)
 7 versus mean (μ_{θ}) for all gridcells combined; (b) the pdf of R^2 values referenced to the
 8 polynomial fit from each coarse-resolution gridcell. [model_moisture_zones_using_coarse_gridcells.m]

9



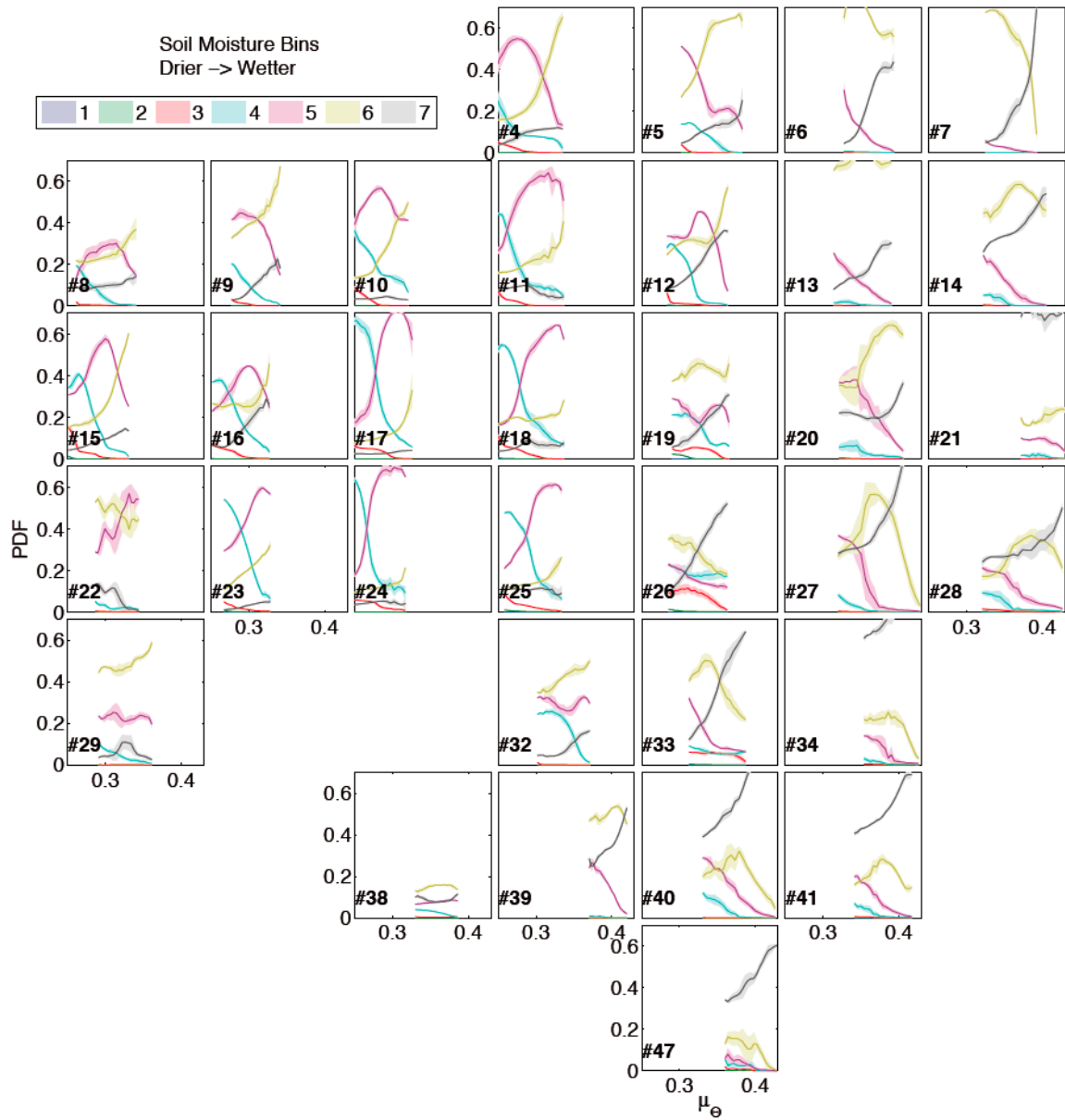
1
2 **Figure 6. Drainage density (length of streams per area) for streams of order 1 and higher.**
3 **Areas with clear convex up shapes for soil moisture variance versus mean tend to be in**
4 **gridcells with higher drainage density. [relate_param_system_properties.m]**



1
 2 **Figure 7.** In each subplot (except for the two in the bottom left hand corner), soil moisture
 3 skewness (s_θ) is plotted versus mean (μ_θ) for that coarse-resolution gridcell based on the
 4 fine-resolution (220 m) model predictions (blue dots) and the best-fit 3rd order polynomial
 5 fits (green line). The individual 7040 m coarse-resolution gridcells are placed in their
 6 relative position in the watershed. Bottom left hand corner: (a) Soil moisture skewness (s_θ)
 7 versus mean (μ_θ) for all gridcells combined; (b) the pdf of R^2 values referenced to the
 8 polynomial fit from each coarse-resolution gridcell. [model_moisture_zones_using_coarse_gridcells.m]

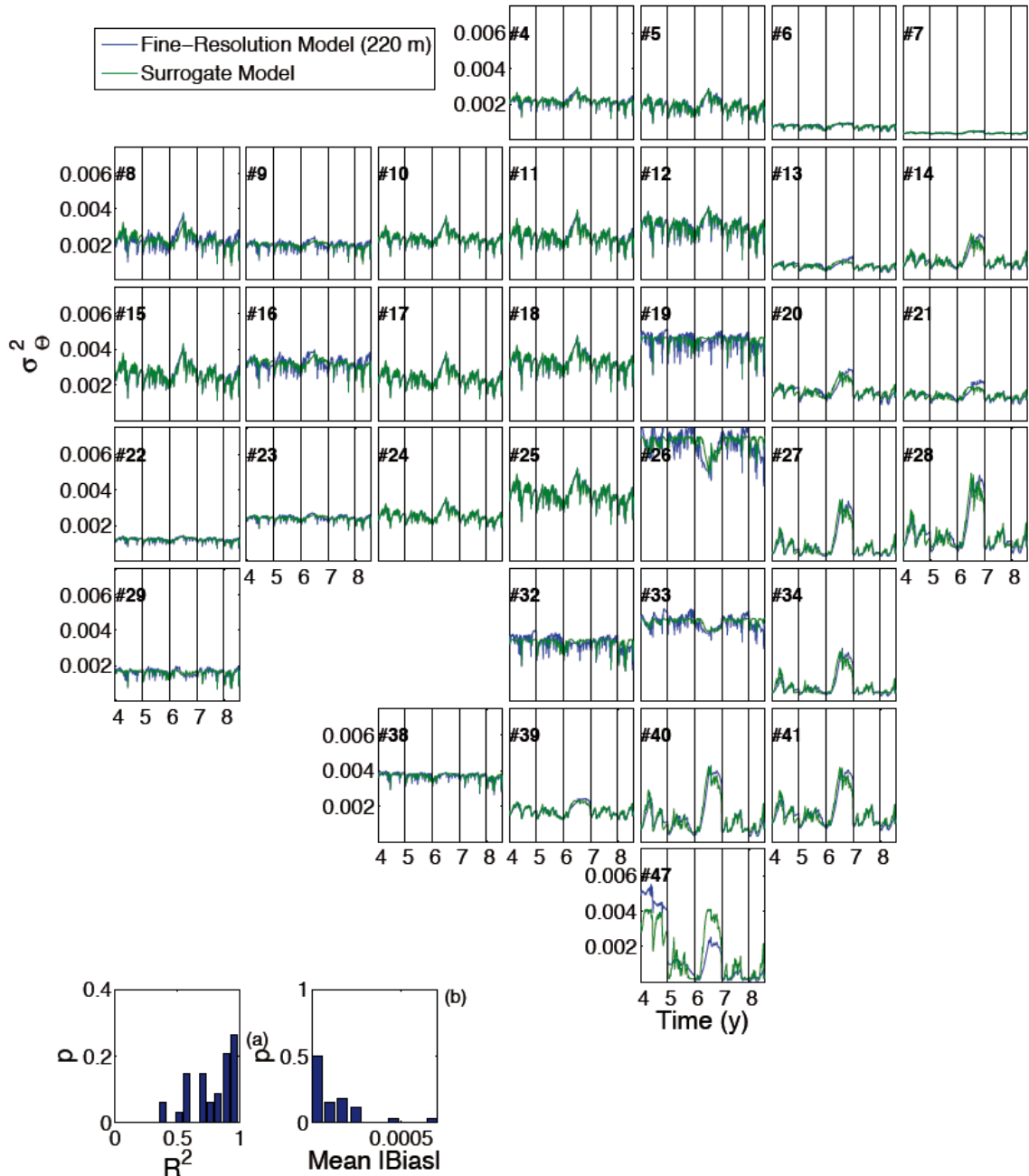
9

1
2



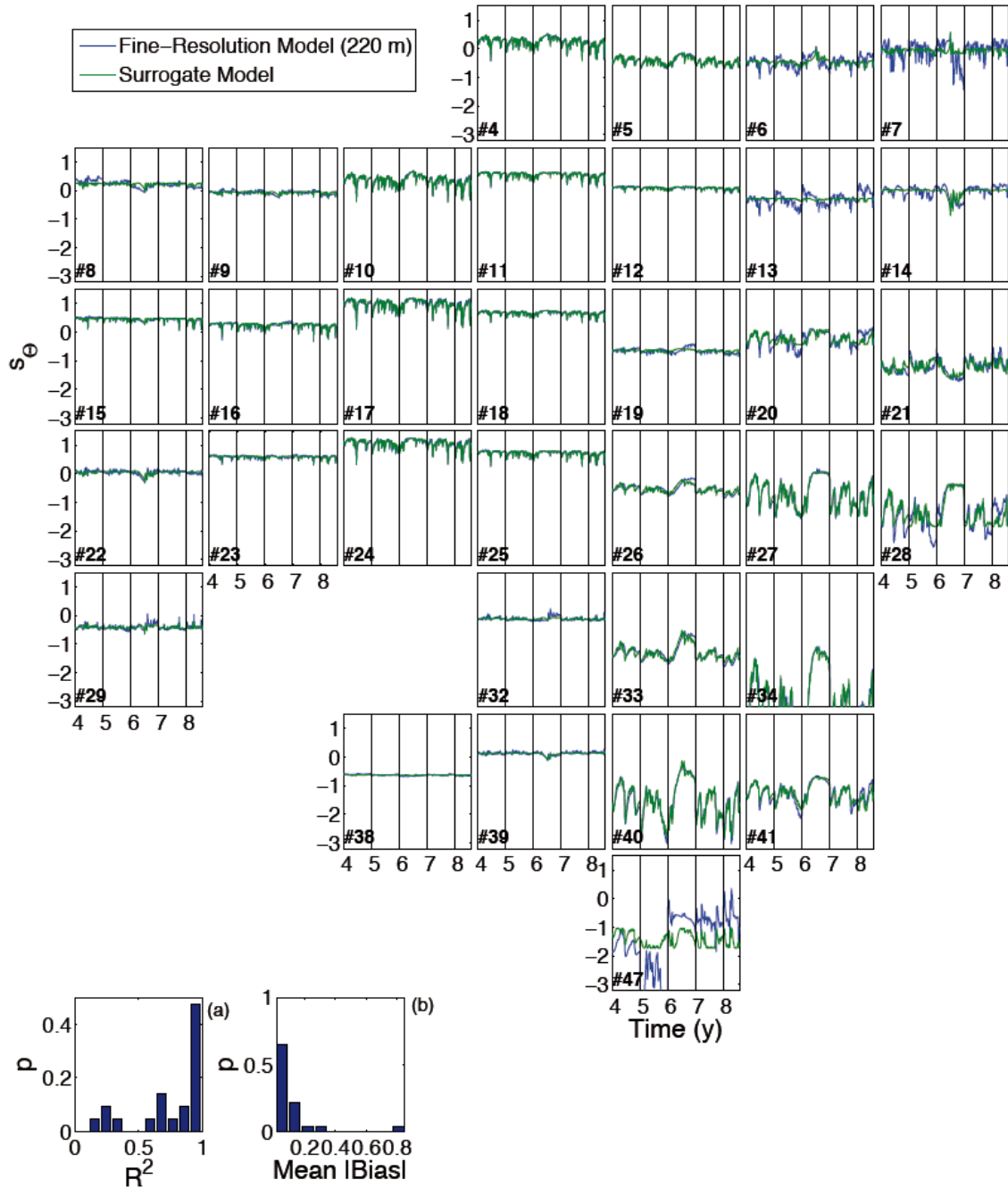
3
4
5
6
7
8

Figure 8. Relationships between mean coarse-resolution gridcell soil moisture (μ_θ) and the proportion of the gridcell in each of ten moisture bins (the wettest seven bins are shown) that span that coarse-resolution gridcell's μ_θ range. The individual 7040 m coarse-resolution gridcells are placed in their relative position in the watershed.



1
 2 **Figure 9. Comparison over time between the fine-resolution (220 m) simulated soil moisture**
 3 **variance (σ_{θ}^2) and that predicted by the surrogate model using the mean of the fine-**
 4 **resolution soil moisture (μ_{θ}). The individual 7040 m coarse-resolution gridcells are placed**
 5 **in their relative position in the watershed. Bottom left hand corner: (a) the pdf of R^2 values**
 6 **between the surrogate model and fine-resolution model predictions of soil moisture variance**
 7 **across all the coarse-resolution gridcells; (b) mean absolute bias between the surrogate and**
 8 **fine-model predictions of soil moisture variance across all the coarse-resolution gridcells.**
 9

[model_moisture_zones_using_coarse_gridcells.m]

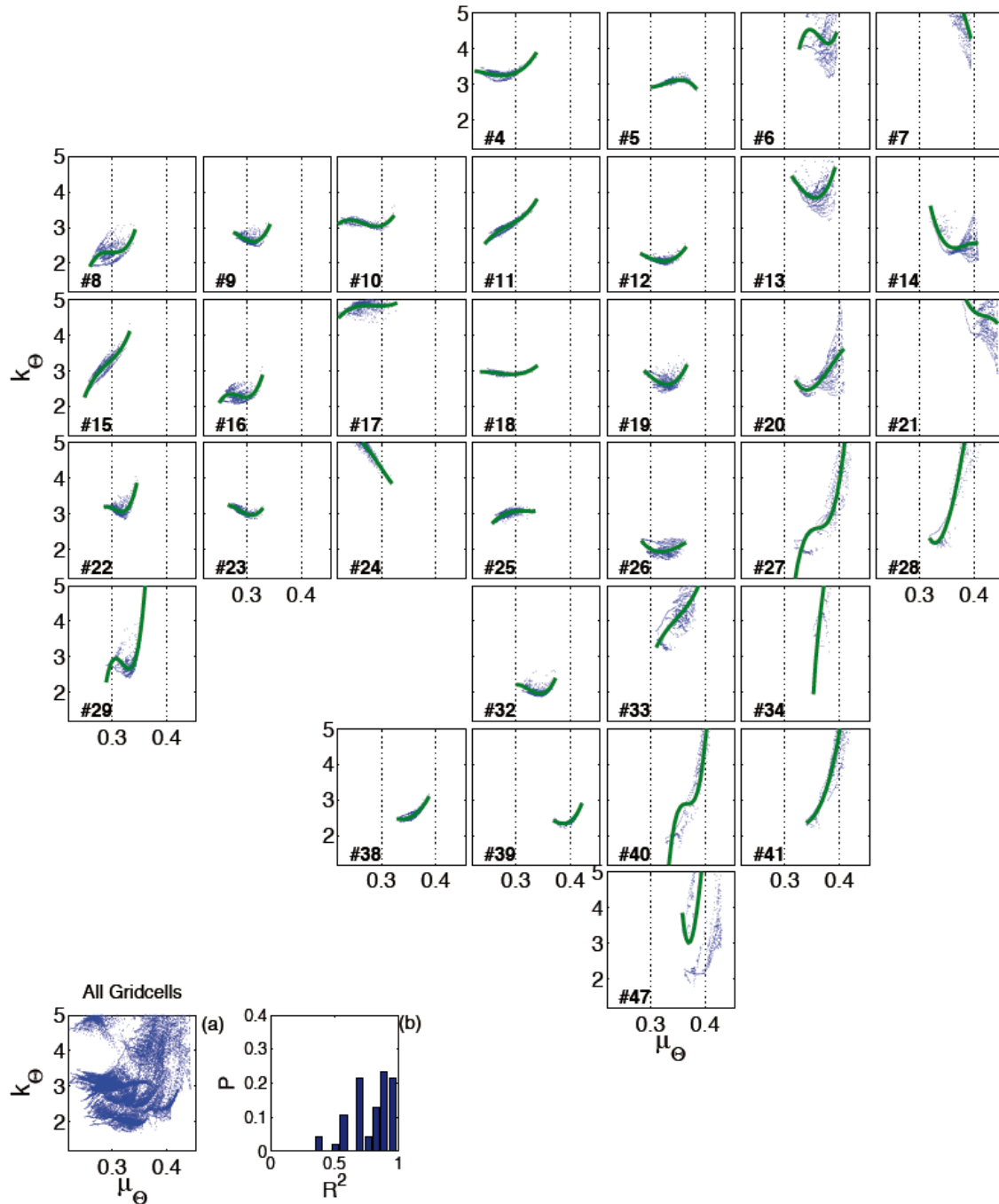


1
 2 **Figure 10.** Comparison over time between the fine-resolution (220 m) simulated soil
 3 moisture skewness (s_θ) and that predicted by the surrogate model using the mean of the
 4 fine-resolution soil moisture (μ_θ). The individual 7040 m coarse-resolution gridcells are
 5 placed in their relative position in the watershed. Bottom left hand corner: (a) the pdf of R^2
 6 values between the surrogate model and fine-resolution model predictions of soil moisture
 7 skewness across all the coarse-resolution gridcells; (b) mean absolute bias between the
 8 surrogate and fine-model predictions of soil moisture skewness across all the coarse-
 9 resolution gridcells. [model_moisture_zones_using_coarse_gridcells.m]

10

1
2
3

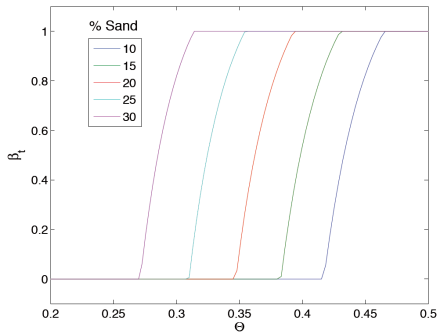
7 Supplemental Material



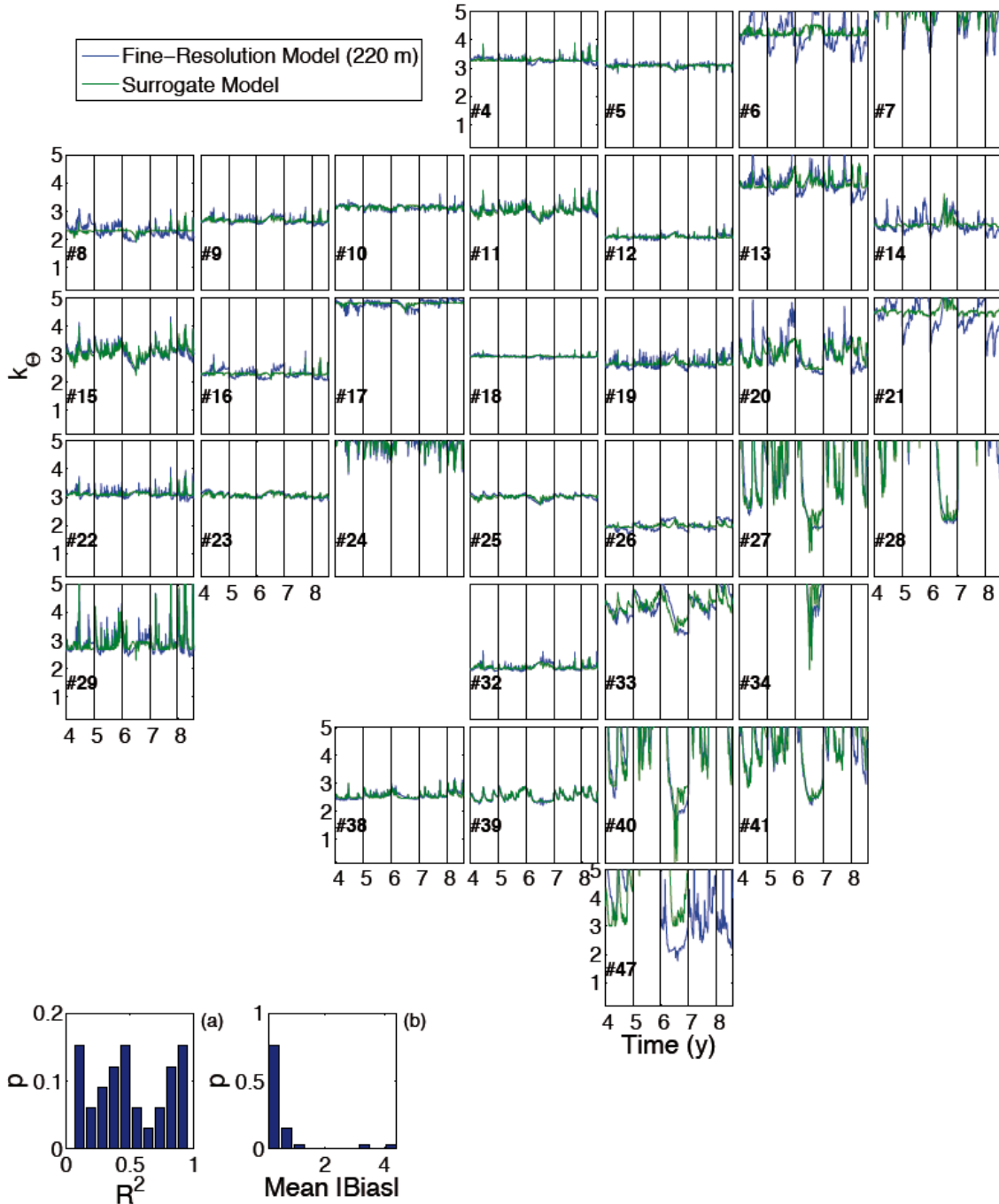
4
5
6
7
8
9

Figure S1. In each subplot (except for the two in the bottom left hand corner), soil moisture kurtosis (k_θ) is plotted versus mean (μ_θ) for that coarse-resolution gridcell based on the fine-resolution (220 m) model predictions (blue dots) and the best-fit 3rd order polynomial fits (green line). The individual 7040 m coarse-resolution gridcells are placed in their relative position in the watershed. Bottom left hand corner: (a) Soil moisture kurtosis (k_θ)

1 versus mean (μ_θ) for all gridcells combined; (b) the pdf of R^2 values referenced to the
2 polynomial fit from each coarse-resolution gridcell. [model_moisture_zones_using_coarse_gridcells.m]
3



4
5 **Figure S2. The water stress term on photosynthesis applied in CLM4 as a function of**
6 **percent sand of the soil.**



1
 2 **Figure S3. Comparison over time between the fine-resolution (220 m) simulated soil**
 3 **moisture kurtosis (k) and that predicted by the surrogate model using the mean of the fine-**
 4 **resolution soil moisture (μ_θ). The individual 7040 m coarse-resolution gridcells are placed**
 5 **in their relative position in the watershed. Bottom left hand corner: (a) the pdf of R^2 values**
 6 **between the surrogate model and fine-resolution model predictions of soil moisture kurtosis**
 7 **across all the coarse-resolution gridcells; (b) mean absolute bias between the surrogate and**
 8 **fine-model predictions of soil moisture kurtosis across all the coarse-resolution gridcells.**
 9 [model_moisture_zones_using_coarse_gridcells.m]

1

2 **8 References**

- 3 Albertson, J. D., and Montaldo, N.: Temporal dynamics of soil moisture variability: 1.
4 Theoretical basis, *Water Resources Research*, 39, Artn 1274, Doi
5 10.1029/2002wr001616, 2003.
- 6 Arrigo, J. A. S., and Salvucci, G. D.: Investigation hydrologic scaling: Observed effects
7 of heterogeneity and nonlocal processes across hillslope, watershed, and regional
8 scales, *Water Resources Research*, 41, Artn W11417, Doi 10.1029/2005wr004032,
9 2005.
- 10 Barrios, M., and Frances, F.: Spatial scale effect on the upper soil effective parameters of
11 a distributed hydrological model, *Hydrological Processes*, 26, 1022-1033, Doi
12 10.1002/Hyp.8193, 2012.
- 13 Brocca, L., Morbidelli, R., Melone, F., and Moramarco, T.: Soil moisture spatial
14 variability in experimental areas of central Italy, *Journal of Hydrology*, 333, 356-
15 373, Doi 10.1016/J.Jhydrol.2006.09.004, 2007.
- 16 Brocca, L., Melone, F., Moramarco, T., and Morbidelli, R.: Spatial-temporal variability
17 of soil moisture and its estimation across scales, *Water Resources Research*, 46, Artn
18 W02516, Doi 10.1029/2009wr008016, 2010.
- 19 Brocca, L., Tullo, T., Melone, F., Moramarco, T., and Morbidelli, R.: Catchment scale
20 soil moisture spatial-temporal variability, *Journal of Hydrology*, 422, 63-75, Doi
21 10.1016/J.Jhydrol.2011.12.039, 2012.
- 22 Burt, T. P., and Pinay, G.: Linking hydrology and biogeochemistry in complex
23 landscapes, *Progress in Physical Geography*, 29, 297-316, Doi
24 10.1191/0309133305pp450ra, 2005.
- 25 Chaplot, V., and Walter, C.: Subsurface topography to enhance the prediction of the
26 spatial distribution of soil wetness, *Hydrological Processes*, 17, 2567-2580, Doi
27 10.1002/Hyp.1273, 2003.
- 28 Choi, M., and Jacobs, J. M.: Spatial soil moisture scaling structure during Soil Moisture
29 Experiment 2005, *Hydrological Processes*, 25, 926-932, Doi 10.1002/Hyp.7877,
30 2011.
- 31 Crave, A., and GascuelOdoux, C.: The influence of topography on time and space
32 distribution of soil surface water content, *Hydrological Processes*, 11, 203-210, Doi
33 10.1002/(Sici)1099-1085(199702)11:2<203::Aid-Hyp432>3.0.Co;2-K, 1997.
- 34 Dai, Z. H., Trettin, C. C., Li, C. S., Li, H., Sun, G., and Amatya, D. M.: Effect of
35 Assessment Scale on Spatial and Temporal Variations in CH₄, CO₂, and N₂O
36 Fluxes in a Forested Wetland, *Water Air Soil Poll*, 223, 253-265, Doi
37 10.1007/S11270-011-0855-0, 2012.
- 38 Das, N. N., and Mohanty, B. P.: Temporal dynamics of PSR-based soil moisture across
39 spatial scales in an agricultural landscape during SMEX02: A wavelet approach,
40 *Remote Sensing of Environment*, 112, 522-534, Doi 10.1016/J.Rse.2007.05.007,
41 2008.
- 42 Dunne, T., and Black, R. D.: Partial Area Contributions to Storm Runoff in a Small New-
43 England Watershed, *Water Resources Research*, 6, 1296-1311, Doi
44 10.1029/Wr006i005p01296, 1970.

1 Famiglietti, J. S., Rudnicki, J. W., and Rodell, M.: Variability in surface moisture content
2 along a hillslope transect: Rattlesnake Hill, Texas, *Journal of Hydrology*, 210, 259-
3 281, Doi 10.1016/S0022-1694(98)00187-5, 1998.

4 Famiglietti, J. S., Devereaux, J. A., Laymon, C. A., Tsegaye, T., Houser, P. R., Jackson,
5 T. J., Graham, S. T., Rodell, M., and van Oevelen, P. J.: Ground-based investigation
6 of soil moisture variability within remote sensing footprints during the Southern
7 Great Plains 1997 (SGP97) Hydrology Experiment, *Water Resources Research*, 35,
8 1839-1851, Doi 10.1029/1999wr900047, 1999.

9 Famiglietti, J. S., Ryu, D. R., Berg, A. A., Rodell, M., and Jackson, T. J.: Field
10 observations of soil moisture variability across scales, *Water Resources Research*,
11 44, Artn W01423, Doi 10.1029/2006wr005804, 2008.

12 Frankenberger, J. R., Brooks, E. S., Walter, M. T., Walter, M. F., and Steenhuis, T. S.: A
13 GIS-based variable source area hydrology model, *Hydrological Processes*, 13, 805-
14 822, Doi 10.1002/(Sici)1099-1085(19990430)13:6<805::Aid-Hyp754>3.0.Co;2-M,
15 1999.

16 Frei, S., Knorr, K. H., Peiffer, S., and Fleckenstein, J. H.: Surface micro-topography
17 causes hot spots of biogeochemical activity in wetland systems: A virtual modeling
18 experiment, *Journal of Geophysical Research-Biogeosciences*, 117, Artn G00n12,
19 Doi 10.1029/2012jg002012, 2012.

20 Gebremichael, M., Rigon, R., Bertoldi, G., and Over, T. M.: On the scaling
21 characteristics of observed and simulated spatial soil moisture fields, *Nonlinear Proc*
22 *Geoph*, 16, 141-150, 2009.

23 Groffman, P. M., Hardy, J. P., Fisk, M. C., Fahey, T. J., and Driscoll, C. T.: Climate
24 Variation and Soil Carbon and Nitrogen Cycling Processes in a Northern Hardwood
25 Forest, *Ecosystems*, 12, 927-943, Doi 10.1007/S10021-009-9268-Y, 2009.

26 GSDD, G. S. D. T.: Global Soil Data Products CD-ROM (IGBP-DIS), Available from
27 Oak Ridge National Laboratory Distributed Active Archive Center, Oak Ridge,
28 Tennessee, U.S.A., 2000.

29 GWIM: State of Michigan Public Act 148 Groundwater Inventory and Mapping Project
30 (GWIM). technical report, 2006.

31 Hu, Z. L., Islam, S., and Cheng, Y. Z.: Statistical characterization of remotely sensed soil
32 moisture images, *Remote Sensing of Environment*, 61, 310-318, Doi 10.1016/S0034-
33 4257(97)89498-9, 1997.

34 Hupet, F., and Vanclooster, M.: Intraseasonal dynamics of soil moisture variability within
35 a small agricultural maize cropped field, *Journal of Hydrology*, 261, 86-101, Pii
36 S0022-1694(02)00016-1, Doi 10.1016/S0022-1694(02)00016-1, 2002.

37 Ivanov, V. Y., Vivoni, E. R., Bras, R. L., and Entekhabi, D.: Catchment hydrologic
38 response with a fully distributed triangulated irregular network model, *Water*
39 *Resources Research*, 40, Artn W11102, Doi 10.1029/2004wr003218, 2004.

40 Ivanov, V. Y., Fatichi, S., Jenerette, G. D., Espeleta, J. F., Troch, P. A., and Huxman, T.
41 E.: Hysteresis of soil moisture spatial heterogeneity and the "homogenizing" effect of
42 vegetation, *Water Resources Research*, 46, Artn W09521, Doi
43 10.1029/2009wr008611, 2010.

44 Jia, Y. W., Wang, H., Zhou, Z. H., and Qiu, Y. Q.: Development of the WEP-L
45 distributed hydrological model and dynamic assessment of water resources in the

1 Yellow River basin, *Journal of Hydrology*, 331, 606-629, Doi
2 10.1016/J.jhydrol.2006.06.006, 2006.

3 Joshi, C., and Mohanty, B. P.: Physical controls of near-surface soil moisture across
4 varying spatial scales in an agricultural landscape during SMEX02, *Water Resources*
5 *Research*, 46, Artn W12503, Doi 10.1029/2010wr009152, 2010.

6 Kollet, S. J., Maxwell, R. M., Woodward, C. S., Smith, S., Vanderborght, J., Vereecken,
7 H., and Simmer, C.: Proof of concept of regional scale hydrologic simulations at
8 hydrologic resolution utilizing massively parallel computer resources, *Water*
9 *Resources Research*, 46, Artn W04201
10 Doi 10.1029/2009wr008730, 2010.

11 Koven, C. D., Riley, W. J., Subin, Z. M., Tang, J. Y., Torn, M. S., Collins, W. D., Bonan,
12 G. B., Lawrence, D. M., and Swenson, S. C.: The effect of vertically resolved soil
13 biogeochemistry and alternate soil C and N models on C dynamics of CLM4,
14 *Biogeosciences*, 10, 7109-7131, Doi 10.5194/Bg-10-7109-2013, 2013.

15 Lawrence, D. M., Oleson, K. W., Flanner, M. G., Thornton, P. E., Swenson, S. C.,
16 Lawrence, P. J., Zeng, X. B., Yang, Z. L., Levis, S., Sakaguchi, K., Bonan, G. B.,
17 and Slater, A. G.: Parameterization Improvements and Functional and Structural
18 Advances in Version 4 of the Community Land Model, *J Adv Model Earth Sy*, 3,
19 Artn M03001, Doi 10.1029/2011ms000045, 2011.

20 Lawrence, J. E., and Hornberger, G. M.: Soil moisture variability across climate zones,
21 *Geophys Res Lett*, 34, Artn L20402, Doi 10.1029/2007gl031382, 2007.

22 Li, B., and Rodell, M.: Spatial variability and its scale dependency of observed and
23 modeled soil moisture over different climate regions, *Hydrology and Earth System*
24 *Sciences*, 17, 1177-1188, Doi 10.5194/Hess-17-1177-2013, 2013.

25 Li, Q., Unger, A. J. A., Sudicky, E. A., Kassenaar, D., Wexler, E. J., and Shikaze, S.:
26 Simulating the multi-seasonal response of a large-scale watershed with a 3D
27 physically-based hydrologic model, *Journal of Hydrology*, 357, 317-336, Doi
28 10.1016/J.jhydrol.2008.05.024, 2008.

29 Lyon, S. W., Walter, M. T., Gerard-Marchant, P., and Steenhuis, T. S.: Using a
30 topographic index to distribute variable source area runoff predicted with the SCS
31 curve-number equation, *Hydrological Processes*, 18, 2757-2771, Doi
32 10.1002/Hyp.1494, 2004.

33 Manfreda, S., McCabe, M. F., Fiorentino, M., Rodriguez-Iturbe, I., and Wood, E. F.:
34 Scaling characteristics of spatial patterns of soil moisture from distributed modelling,
35 *Adv Water Resour*, 30, 2145-2150, Doi 10.1016/J.Advwatres.2006.07.009, 2007.

36 Markstrom, S. L., Niswonger, R. G., Regan, R. S., Prudic, D. E., and Barlow, P. M.:
37 GSFLOW-Coupled Ground-water and Surface-water FLOW model based on the
38 integration of the Precipitation-Runoff Modeling System (PRMS) and the Modular
39 Ground-Water Flow Model (MODFLOW-2005), U.S. Geological Survey, Reston,
40 VA, USA, 240, 2008.

41 Mascaro, G., Vivoni, E. R., and Deidda, R.: Downscaling soil moisture in the southern
42 Great Plains through a calibrated multifractal model for land surface modeling
43 applications, *Water Resources Research*, 46, Artn W08546, Doi
44 10.1029/2009wr008855, 2010.

1 Mascaro, G., Vivoni, E. R., and Deidda, R.: Soil moisture downscaling across climate
2 regions and its emergent properties, *JOURNAL OF GEOPHYSICAL RESEARCH-*
3 *ATMOSPHERES*, 116, Artn D22114, Doi 10.1029/2011jd016231, 2011.

4 Maxwell, R. M.: Infiltration in Arid Environments: Spatial Patterns between Subsurface
5 Heterogeneity and Water-Energy Balances, *Vadose Zone Journal*, 9, 970-983, Doi
6 10.2136/Vzj2010.0014, 2010.

7 Maxwell, R. M., Putti, M., Meyerhoff, S., Delfs, J.-O., Ferguson, I. M., Ivanov, V., Kim,
8 J., Kolditz, O., Kollet, S. J., Kumar, M., Lopez, S., Niu, J., Paniconi, C., Park, Y.-J.,
9 Phanikumar, M. S., Shen, C., Sudicky, E. A., and Sulis, M.: Surface-subsurface
10 model intercomparison: A first set of benchmark results to diagnose integrated
11 hydrology and feedbacks, *Water Resour. Res.*, doi:10.1002/2013WR013725, 2014.

12 McClain, M. E., Boyer, E. W., Dent, C. L., Gergel, S. E., Grimm, N. B., Groffman, P.
13 M., Hart, S. C., Harvey, J. W., Johnston, C. A., Mayorga, E., McDowell, W. H., and
14 Pinay, G.: Biogeochemical hot spots and hot moments at the interface of terrestrial
15 and aquatic ecosystems, *Ecosystems*, 6, 301-312, Doi 10.1007/S10021-003-0161-9,
16 2003.

17 McMichael, C. E., Hope, A. S., and Loaiciga, H. A.: Distributed hydrological modelling
18 in California semi-arid shrublands: MIKE SHE model calibration and uncertainty
19 estimation, *Journal of Hydrology*, 317, 307-324, Doi 10.1016/J.Jhydrol.2005.05.023,
20 2006.

21 MDNR: 2001 IFMAP/GAP Lower Peninsula Land Cover, available at
22 [http://www.mcgi.state.mi.us/mgdl/?rel=thext&action=thmname&cid=5&cat=Land+](http://www.mcgi.state.mi.us/mgdl/?rel=thext&action=thmname&cid=5&cat=Land+Cover+2001)
23 [Cover+2001](http://www.mcgi.state.mi.us/mgdl/?rel=thext&action=thmname&cid=5&cat=Land+Cover+2001), retrieved 2009-Nov-28, Michigan Department of Natural Resources,
24 2010.

25 Merot, P., Ezzahar, B., Walter, C., and Arousseau, P.: Mapping Waterlogging of Soils
26 Using Digital Terrain Models, *Hydrological Processes*, 9, 27-34, Doi
27 10.1002/Hyp.3360090104, 1995.

28 Miguez-Macho, G., and Fan, Y.: The role of groundwater in the Amazon water cycle: 1.
29 Influence on seasonal streamflow, flooding and wetlands, *JOURNAL OF*
30 *GEOPHYSICAL RESEARCH-ATMOSPHERES*, 117, Artn D15113, Doi
31 10.1029/2012jd017539, 2012.

32 Montaldo, N., and Albertson, J. D.: Temporal dynamics of soil moisture variability: 2.
33 Implications for land surface models, *Water Resources Research*, 39, Artn 1275, Doi
34 10.1029/2002wr001618, 2003.

35 Moore, I. D., Burch, G. J., and Mackenzie, D. H.: Topographic Effects on the
36 Distribution of Surface Soil-Water and the Location of Ephemeral Gullies, *T Asae*,
37 31, 1098-1107, 1988.

38 Moore, I. D., Norton, T. W., and Williams, J. E.: Modeling Environmental Heterogeneity
39 in Forested Landscapes, *Journal of Hydrology*, 150, 717-747, Doi 10.1016/0022-
40 1694(93)90133-T, 1993.

41 NCDC: National Climatic Data Center, 2010.

42 Niu, G. Y., Paniconi, C., Troch, P. A., Scott, R. L., Durcik, M., Zeng, X., Huxman, T. E.,
43 and Goodrich, D. C.: An integrated modelling framework of catchment-scale
44 ecohydrological processes: 1. Model description and tests over an energy-limited
45 watershed, submitted *Ecohydrology*, 2013.

1 Niu, J., and Phanikumar, M. S.: Quantifying Fluxes of Chemical and Biological Species
2 in Great Lakes Watersheds: A Reactive Transport Modeling Framework, American
3 Geophysical Union Annual Fall Meeting, San Francisco, CA, 2012,
4 Nykanen, D. K., and Foufoula-Georgiou, E.: Soil moisture variability and scale-
5 dependency of nonlinear parameterizations in coupled land-atmosphere models, *Adv*
6 *Water Resour*, 24, 1143-1157, Doi 10.1016/S0309-1708(01)00046-X, 2001.
7 Pan, F., and Peters-Lidard, C. D.: On the relationship between mean and variance of soil
8 moisture fields, *Journal of the American Water Resources Association*, 44, 235-242,
9 Doi 10.1111/J.1752-1688.2007.00150.X, 2008.
10 Park, S. J., and van de Giesen, N.: Soil-landscape delineation to define spatial sampling
11 domains for hillslope hydrology, *Journal of Hydrology*, 295, 28-46, Doi
12 10.1016/J.jhydrol.2004.02.022, 2004.
13 Qiu, Y., Fu, B. J., Wang, J., and Chen, L. D.: Soil moisture variation in relation to
14 topography and land use in a hillslope catchment of the Loess Plateau, China,
15 *Journal of Hydrology*, 240, 243-263, Doi 10.1016/S0022-1694(00)00362-0, 2001.
16 Qu, Y. Z., and Duffy, C. J.: A semidiscrete finite volume formulation for multiprocess
17 watershed simulation, *Water Resources Research*, 43, Artn W08419, Doi
18 10.1029/2006wr005752, 2007.
19 Rigon, R., Bertoldi, G., and Over, T. M.: GEOTop: A distributed hydrological model with
20 coupled water and energy budgets, *Journal of Hydrometeorology*, 7, 371-388, Doi
21 10.1175/Jhm497.1, 2006.
22 Rodriguez-Iturbe, I., Vogel, G. K., Rigon, R., Entekhabi, D., Castelli, F., and Rinaldo, A.:
23 On the Spatial-Organization of Soil-Moisture Fields, *Geophys Res Lett*, 22, 2757-
24 2760, Doi 10.1029/95gl02779, 1995.
25 Rosenbaum, U., Bogena, H. R., Herbst, M., Huisman, J. A., Peterson, T. J., Weuthen, A.,
26 Western, A. W., and Vereecken, H.: Seasonal and event dynamics of spatial soil
27 moisture patterns at the small catchment scale, *Water Resources Research*, 48, Artn
28 W10544, Doi 10.1029/2011wr011518, 2012.
29 Ryu, D., and Famiglietti, J. S.: Characterization of footprint-scale surface soil moisture
30 variability using Gaussian and beta distribution functions during the Southern Great
31 Plains 1997 (SGP97) hydrology experiment, *Water Resources Research*, 41, Artn
32 W12433, Doi 10.1029/2004wr003835, 2005.
33 Salvucci, G. D., and Entekhabi, D.: Hillslope and Climatic Controls on Hydrologic
34 Fluxes, *Water Resources Research*, 31, 1725-1739, Doi 10.1029/95wr00057, 1995.
35 Schwanghart, W., and Kuhn, N. J.: TopoToolbox: A set of Matlab functions for
36 topographic analysis, *Environ Modell Softw*, 25, 770-781, Doi
37 10.1016/J.Envsoft.2009.12.002, 2010.
38 Seyfried, M.: Spatial variability constraints to modeling soil water at different scales,
39 *Geoderma*, 85, 231-254, Doi 10.1016/S0016-7061(98)00022-6, 1998.
40 Shen, C.: A process-based distributed hydrologic model and its application to a Michigan
41 watershed, Ph.D., Civil and Environmental Engineering, Michigan State University,
42 East Lansing, MI, 270 pp., 2009.
43 Shen, C., Niu, J., and Phanikumar, M. S.: PAWS+CLM: A Computationally Efficient
44 Framework for Linking Hydrologic and Ecosystem Processes with GIS Data
45 Integration Capabilities in review *Environmental Modeling and Software*, 2013a.

- 1 Shen, C., Niu, J., and Phanikumar, M. S.: Evaluating controls on coupled hydrologic and
2 vegetation dynamics in a humid continental climate watershed using a subsurface -
3 land surface process model, *Water Resources Research*, 49, doi:10.1002/wrcr.20189,
4 2013b.
- 5 Shen, C. P., and Phanikumar, M. S.: A process-based, distributed hydrologic model based
6 on a large-scale method for surface-subsurface coupling, *Adv Water Resour*, 33,
7 1524-1541, Doi 10.1016/J.Advwatres.2010.09.002, 2010.
- 8 Simard, A.: Predicting groundwater flow and transport using Michigan's statewide
9 wellogic database, PhD, Civil and Environmental Engineering, Michigan State
10 University, East Lansing, MI, 2007.
- 11 Sivandran, G., and Bras, R. L.: Dynamic root distributions in ecohydrological modeling:
12 A case study at Walnut Gulch Experimental Watershed, *Water Resources Research*,
13 49, 3292-3305, Doi 10.1002/Wrcr.20245, 2013.
- 14 Subin, Z. M., Riley, W. J., Jin, J., Christianson, D. S., Torn, M. S., and Kueppers, L. M.:
15 Ecosystem Feedbacks to Climate Change in California: Development, Testing, and
16 Analysis Using a Coupled Regional Atmosphere and Land Surface Model (WRF3-
17 CLM3.5), *Earth Interactions*, 15, Artn 15, Doi 10.1175/2010ei331.1, 2011.
- 18 Tague, C., Band, L., Kenworthy, S., and Tenebaum, D.: Plot- and watershed-scale soil
19 moisture variability in a humid Piedmont watershed, *Water Resources Research*, 46,
20 Artn W12541, Doi 10.1029/2009wr008078, 2010.
- 21 Tang, J. Y., Riley, W. J., Koven, C. D., and Subin, Z. M.: CLM4-BeTR, a generic
22 biogeochemical transport and reaction module for CLM4: model development,
23 evaluation, and application, *Geoscientific Model Development*, 6, 127-140, Doi
24 10.5194/Gmd-6-127-2013, 2013.
- 25 Teuling, A. J., and Troch, P. A.: Improved understanding of soil moisture variability
26 dynamics, *Geophys Res Lett*, 32, Artn L05404, Doi 10.1029/2004gl021935, 2005.
- 27 Teuling, A. J., Hupet, F., Uijlenhoet, R., and Troch, P. A.: Climate variability effects on
28 spatial soil moisture dynamics, *Geophys Res Lett*, 34, Artn L06406, Doi
29 10.1029/2006gl029080, 2007.
- 30 Vereecken, H., Kamai, T., Harter, T., Kasteel, R., Hopmans, J., and Vanderborght, J.:
31 Explaining soil moisture variability as a function of mean soil moisture: A stochastic
32 unsaturated flow perspective, *Geophys Res Lett*, 34, Artn L22402, Doi
33 10.1029/2007gl031813, 2007.
- 34 Vivoni, E. R., Entekhabi, D., Bras, R. L., and Ivanov, V. Y.: Controls on runoff
35 generation and scale-dependence in a distributed hydrologic model, *Hydrology and
36 Earth System Sciences*, 11, 1683-1701, 2007.
- 37 Vivoni, E. R., Rodriguez, J. C., and Watts, C. J.: On the spatiotemporal variability of soil
38 moisture and evapotranspiration in a mountainous basin within the North American
39 monsoon region, *Water Resources Research*, 46, Artn W02509, Doi
40 10.1029/2009wr008240, 2010.
- 41 Weill, S., Mazzia, A., Putti, M., and Paniconi, C.: Coupling water flow and solute
42 transport into a physically-based surface-subsurface hydrological model, *Adv Water
43 Resour*, 34, 128-136, Doi 10.1016/J.Advwatres.2010.10.001, 2011.
- 44 Western, A. W., Grayson, R. B., Bloschl, G., Willgoose, G. R., and McMahon, T. A.:
45 Observed spatial organization of soil moisture and its relation to terrain indices,
46 *Water Resources Research*, 35, 797-810, Doi 10.1029/1998wr900065, 1999.

- 1 Williams, A. G., Ternan, J. L., Fitzjohn, C., de Alba, S., and Perez-Gonzalez, A.: Soil
2 moisture variability and land use in a seasonally arid environment, *Hydrological*
3 *Processes*, 17, 225-235, Doi 10.1002/Hyp.1120, 2003.
- 4 Wilson, D. J., Western, A. W., and Grayson, R. B.: Identifying and quantifying sources
5 of variability in temporal and spatial soil moisture observations, *Water Resources*
6 *Research*, 40, Artn W02507, Doi 10.1029/2003wr002306, 2004.
- 7 Wood, E. F.: Effects of soil moisture aggregation on surface evaporative fluxes, *Journal*
8 *of Hydrology*, 190, 397-412, Doi 10.1016/S0022-1694(96)03135-6, 1997.
- 9 Wood, E. F.: Scale analyses for land-surface hydrology, in: *Scale Dependence and Scale*
10 *Invariance in Hydrology*, edited by: Sposito, G., Cambridge University Press,
11 Cambridge, UK, 1-29, 1998.
- 12 Wood, E. F., Roundy, J. K., Troy, T. J., van Beek, L. P. H., Bierkens, M. F. P., Blyth, E.,
13 de Roo, A., Doll, P., Ek, M., Famiglietti, J., Gochis, D., van de Giesen, N., Houser,
14 P., Jaffe, P. R., Kollet, S., Lehner, B., Lettenmaier, D. P., Peters-Lidard, C.,
15 Sivapalan, M., Sheffield, J., Wade, A., and Whitehead, P.: Hyperresolution global
16 land surface modeling: Meeting a grand challenge for monitoring Earth's terrestrial
17 water, *Water Resources Research*, 47, Artn W05301, Doi 10.1029/2010wr010090,
18 2011.
- 19 Zhang, Y., Sachs, T., Li, C. S., and Boike, J.: Upscaling methane fluxes from closed
20 chambers to eddy covariance based on a permafrost biogeochemistry integrated
21 model, *Global Change Biology*, 18, 1428-1440, Doi 10.1111/J.1365-
22 2486.2011.02587.X, 2012.
- 23